General Disclaimer

One or more of the Following Statements may affect this Document

- This document has been reproduced from the best copy furnished by the organizational source. It is being released in the interest of making available as much information as possible.

- This document may contain data, which exceeds the sheet parameters. It was furnished in this condition by the organizational source and is the best copy available.

- This document may contain tone-on-tone or color graphs, charts and/or pictures, which have been reproduced in black and white.

- This document is paginated as submitted by the original source.

- Portions of this document are not fully legible due to the historical nature of some of the material. However, it is the best reproduction available from the original submission.

Mobil Tyco Solar Energy Corporation
16 Hickory Drive
Waltham, Massachusetts 02154

LARGE AREA SILICON SHEET BY EFG

Program Manager: F.V. Wald

Fourth Quarterly Report - Subcontract No. 954355

Covering Period: October 1, 1978 - December 31, 1978

March 1, 1979

Page intentionally left blank

ABSTRACT

Growth station no. 1 further explored displaced die concepts during this quarter, along with some initial work on buckle characterization. This work will continue. Also, convective impurity redistribution was further studied. In particular, a side channel die was used to grow material doped with aluminum and compare the results at least semiquantitaively with computer calculations. The ribbons grown have not been characterized yet.

In station no. 3A growth from single cartridges was continued to create a quality baseline to allow comparison of the results with those in the upcoming multiple run and to choose the most appropriate die design. Also fabrication and assembly work on the actual five ribbon furnace continued.

On furnace 17 progress was made toward the development of the video optical system for edge position and meniscus height control. Also, in preparation for a detailed program, designed to explore the buckling problem, ribbon guidance in the machine was improved. Buckle free, full width ribbon was then grown under stable conditions without a cold shoe, an achievement essential to finally arrive at quantitative correlations between growth conditions and buckle formation.

The most significant result from the characterization program was a demonstration that the original runs with displaced dies were indeed reproducible, inasmuch as large area cells (7.5 x 7.5 cm^2) of ~9% efficiency could be fabricated again from run 18-103, a repeat of run no. 18-102 which had previously produced the best cells.

TABLE OF CONTENTS

LIST OF TABLES

Table of Contents (continued)

LIST OF FIGURES

I. INTRODUCTION

At the beginning of fiscal year 1978, it was well established that EFG material, in spite of its imperfect nature, is quite capable of producing large area (2.5×10 cm^2) solar cells with efficiencies of at least 12%. Indeed, the discussion of whether small area cells of higher efficiency could conceivably be prepared from some of the material had already been shifting to the question of defining the influence of particular defects on the overall yield of cells prepared from whole multiple meter lengths of ribbon, and attempts to prepare single cells with optimized properties were de-emphasized.

Instead, under this contract the focus shifted to considering even larger cells (5×10 cm^2 and 7.5×7.5 cm^2) prepared from 5 cm and 7.5 cm wide ribbon, grown under conditions which would make high rate multiple ribbon growth a practical reality. The characterization task, therefore, took more and more of an interest in questions related to uniformity of properties over very large cell areas and within long ribbons, instead of concerning itself with the top performance of selected small ribbon areas.

Thus, the program in its philosophy shifted to engineering research, i.e., answering questions related to specific machine design elements; the ribbon quality to be expected from growth stations built in certain ways and using particular materials of construction, and the relations between silicon ribbon quality and productivity; i.e., such questions as to how speed and width affect the ribbon properties both from a mechanical (flatness, thickness uniformity, etc.) and solid-state (in the end, solar cell efficiency) standpoint.

Overall, we believe that this programmatic approach has been successful and that a realistic engineering concept has been proven which will allow the achievement of high ribbon productivity along with good ribbon quality and thus low solar cell blank cost. Specifically, major achieve-

ments of the program which support this statement are:

1. The soundness of the engineering concepts has been demonstrated by the achievement of multiple (five) ribbon growth for periods up to 20 hours.

2. Significantly improved single ribbon equipment using a cartridge (Machine 17) has been constructed on schedule this year. It provides unique capabilities for studying and understanding the growth process itself as well as a simple basic concept for automatic feedback control.

3. The work on JPL Machine No. 1 (MTSEC No. 18) has led to the design of highly reliable growth cartridges in which experiments of 7.5 cm wide growth can be conducted in a reproducible manner, i.e., when one sets out to grow a ribbon, one can actually grow as much as a full crucible allows every time. During the last three months, this equipment operated on a regular schedule of two one-day runs per week, without any significant parts failure.

4. The introduction of the so-called "mini cold shoe" represents a major advance in reliable cartridge design.

5. A concept that had been proposed for some time, namely to use specific interface shaping to improve material properties of wide ribbon, has finally been reduced to practicability by the use of displaced dies. This has led to solar cells (in sizes of 2.5×10 cm^2, 2.5×7.5 cm^2, and 7.5×7.5 cm^2) grown from a reliable, practical cartridge system which have average efficiencies of over 9% in random lots of ~10 pieces. Most importantly, the material is indeed asymmetrical as predicted, not only with respect to solar cell efficiency but also with respect to silicon carbide density.

Thus, enough understanding of the effects has been gained to make further advances in this area quite likely so that the solar cell efficiency in these large ribbon cells is expected to reach similar averages which are now obtained in cells made from smaller ribbons.

6. Detailed studies of the effect of the gaseous environment in an EFG furnace have led to the discovery that growth stability can be significantly enhanced and SiC density can be greatly reduced by proper atmosphere control.

However, before final production machine prototype design can begin, the various approaches which have been derived need still to be optimized and made ready for fully automatic operation at high growth rates, a fact

that becomes clearly apparent from the detailed discussions in the text
that follows. In particular, the main hurdle toward higher growth rates,
namely the buckling that produces unacceptable, non-flat ribbon, has to
be overcome and the approaches toward higher cell efficiencies have to
be refined so that they are more effective and can be combined with high
growth rates (>5 cm/min).

Experiments which generate the needed basic facts in these areas
can, however, be conducted now in an optimum way, since both direct ob-
servational tools (Machine 17) and sufficient basic understanding of
the details of the growth process are available. We are thus confident
that the final prototype design of a ribbon production machine could
begin within a year.

II. WORK ON CRYSTAL GROWTH STATION NO. 1 by J. P. Kalejs

A. Overview

The experiments carried out in this quarter have extended earlier work on the study of the influence of deliberately induced thermal asymmetries on ribbon growth conditions and material quality. Growth has been attempted with asymmetric face heater and die top shield configurations, and reverse radius dies, in order to improve growth conditions with increased die displacements (up to 0.025 cm).

Growth runs have been made from quartz crucibles to add to baseline data on differences between quartz and graphite crucible-grown material. Buckle characterization with respect to type, period, and amplitude has been initiated to gather data for the standard 7.5 cm cartridge system in the speed range from 3 to 4 cm/min. The study of convective impurity redistribution has been continued with growth from side channel dies from both undoped melts and melts doped with aluminum.

B. Experimental

The efforts during this reporting period have consisted of a continuation of growth to establish baseline quality levels for ribbon grown from graphite and quartz crucibles and of further testing of displaced die designs. The run data are summarized in Table I. Growth from what is considered to be the optimum die configuration tested to date, the displaced central capillary die, was used in run 18-103, a repeat of run 18-102. Together, the solar cell data from these two runs show a predominance of material from graphite crucibles capable of producing solar cells in the range from 9 to 10%, AM1 conditions and AR coated. Comparison of material grown from quartz crucibles in runs 18-105 and 18-106 shows that lower efficiencies than those for material grown from graphite crucibles have resulted. This does not reflect the trends observed in JPL No. 3A, where quartz-grown material appears to yield higher

Table I. Run and Ribbon Data for JPL No. 1. All-molybdenum Cold Shoe Used in Runs 18-103 to 18-105, Stretched Version of 5 cm Cold Shoes in All Others. Cold Shoe Spacing was 0.32 cm in the former, and 0.16 in the Latter.

Run No.	Speed (cm/min)	Length (m)	Comments
18-103	2.5 - 3.5	2.9	Repeat of 18-102; central capillary displaced die.
18-104	2.5 - 3.5	1.6	First test of asymmetric face heater and 0.025 cm displaced die with 0.050 cm top slot. Full-width growth not possible due to end instabilities.
18-105	2.5 - 3.9	2.6	First quartz crucible run in this clean series; central capillary die, no displacement.
18-106	2.5 - 3.6	2.8	Second quartz crucible run in this clean series; central capillary displaced die: 0.012 cm displacement on 0.050 cm top slot. Stretched version of 5 cm cold shoe blocks and heat removal elements.
18-107	-	-	Repeat of 18-106. No growth possible due to silicon flood from cracked quartz crucible.
18-108	3.0 - 3.6	1.3	First test of asymmetric die top shield; cold shoe as in 18-107. Poor growth conditions, narrow ribbon (~2.5 cm) growth only.
18-109	3.5 - 4.3	3.4	First test of 0.025 cm displaced die with reverse 1.25 m radius superimposed. Reasonable growth, most stable below 4.0 cm/min.
18-110	3.0 - 3.8	1.2	Repeat of 18-109. Cold main zone limited growth output.
18-111	2.9 - 4.3	2.0	First test of side channel die, 0.020 cm top slot. Silicon flood in main zone limited growth. Thick ribbon, due partly to splaying of die ends. Undoped melt.
18-112	3.0 - 3.4	2.2	Undoped run for evaluation of residual impurity redistribution with 0.005 cm displacement central capillary die. Excellent growth conditions.
18-113	3.2 - 4.4	2.7	Repeat of 18-111 with 1 Ω-cm boron doped melt. No problems with ends of die.
18-115	2.8 - 3.7	3.0	Repeat of 18-111 with 3 Ω-cm aluminum doped melt. Good growth conditions, crucible emptied.
18-116	-	-	Test of 2 cm coverage end heaters. Growth not possible due to thermal imbalance across die top.

performance solar cells than that grown from graphite crucibles.[1] The reasons for this discrepancy are not evident at this time, and further work is planned in this area.

Experimentation with displaced dies has been continued in order to gain understanding of the effect of displacement on material quality and also to search for die configurations with increased displacements allowing stable and reliable growth. Acceptable growth conditions with displaced dies have been obtained for displacements of less than 0.012 cm, while steady-state, full-width growth has been limited to speeds of less than about 3.5 cm/min.[1] At higher speeds and/or greater displacements, deterioration in growth stability was generally noticeable in the form of ribbon edge wandering and inability to maintain width during increases in growth speed. For example, growth with a 0.025 cm displacement was tried in run 18-95, but conditions were found to be unsatisfactory as edge instabilities confined growth to ribbon less than 5 cm wide. Modifications in cartridge components in close proximity to the die top as well as in the die top contour shape were tested in an attempt to address this problem. The results of these tests will now be described.

Two modifications of cartridge components designed to introduce thermal asymmetry across the ribbon thickness have been subsequently investigated to attempt to improve this situation. In run 18-104, a regular face heater was thinned on one side to reduce the cross-section by about 40% relative to the other side. It was then installed with the thinner, higher resistance, side along the displaced die face. The level of heating of the undisplaced die face was consequently increased relative to the displaced face. Growth conditions with this asymmetric heater were not noticeably improved over the earlier run with the 0.025 cm displacement, and only narrow ribbon could be grown stably once more. A parallel effort to introduce thermal asymmetry was made in run 18-108, in the use of a die top shield modified to be asymmetrically located with respect to the die faces. Growth conditions with the 0.025 cm displacement die again were not noticeably different from those encountered in the two earlier runs. It was concluded on the basis of these experiments that modifications of cartridge components below the level of the die top and growth interface do not have a first order effect insofar as ease of growth is concerned. The material grown will be examined for property changes that could be attributed to thermal asymmetries resulting from the component modifications detailed.

7

An alternate approach in the effort to increase growth stability
with larger die displacements was to shape the die top. For simplicity,
the first case that was tried was a straightforward contouring of the
displaced die by a radius. A 0.025 cm displaced die (and 0.050 cm top
slot) was remachined, superimposing a reverse or "frowning" radius of
1.25 m on the displacement. This resulted in a graduated displacement
die, with the displacement varying from 0.025 cm at the center to zero
at the edges.

The reverse radius displaced die was used in runs 18-109 and 18-110
(see Table I). Growth conditions were satisfactory in both runs, and
nearly full-width (6.5 to 7.0 cm wide) ribbon was grown at speeds up to
4.3 cm/min. The speed range over which stable growth conditions were
realized was generally greater than that available without the radius.
This is attributed to the increased range of meniscus heights at the die
ends made available by the wider die top flats. Growth conditions were
judged to be less than optimal in these preliminary runs, and additional
evaluation will be needed, particularly in the area of material quality
improvement, to establish the utility of this type of die design.

A study of convective impurity redistribution has been started using
a side channel die. The design of this die reverses the melt flow
pattern of the central capillary die in that the capillary feed channels
are formed by 0.050 cm wide saw cuts extending 1.25 cm deep into each
end of the die, in addition to the usual 0.050 cm wide and 0.25 cm deep
die top slot across the die width. This configuration is expected to
result in segregated impurities being preferentially redistributed to
the center of the growing ribbon by melt convection. In this location,
their effect on material quality and solar cell performance will be
easier to evaluate than at the edges, which are often inconsistently
treated during characterization.

Three runs have been made with the side channel die: with an un-
doped melt (18-111); with the regular boron doping to 1 Ω-cm (18-113);
and with a 3 Ω-cm aluminum doped melt (18-115). Growth conditions in all
three cases were satisfactory, although some splaying of the die ends
was experienced in run 18-111. Ribbon edge stability was generally poor,
especially at full width and at higher speeds (above 3.5 cm/min). It is
suspected that the melt heats the die ends more than the center with
this capillary configuration, and that this acts to decrease temperature
gradients at the die edges and so reduce their effectiveness in aiding
stability. The material grown in these three runs will be evaluated and
compared for evidence of impurity redistribution.

Future work in JPL No. 1 in the next quarter will center around a third series of clean runs. The furnace is to be cleaned and main zone and cartridge components replaced in preparation for them. As in the initial series, one set of main zone molybdenum shields was used throughout the second series of clean runs, extending from 18-90 to 18-116, and these stood up reasonably well. However, deterioration of their insulating capability was noticeable as the series progressed. This resulted in one run, 18-110, being carried out with a partially frozen melt. The problem was rectified in later runs by raising the melt temperature $25^\circ C$.

A departure in the third series of clean runs will be made insofar as system construction materials are concerned. The molybdenum main zone shields will be replaced by graphite fiberform insulation. A parallel effort to replace some molybdenum shields in the cartridge by graphite will also be made. These changes are thought to be desirable for two reasons. First, the effect of graphite insulation on growth stability, as compared to the molybdenum shields, will be evaluated. The main zone shielding is one major difference found between JPL No. 1 and No. 3A, and thus this question is of some concern in a comparison of the two furnaces. Second, the effect of the removal of large surface areas of molybdenum, with their potential for providing contaminating oxides and impurities, will be evaluated insofar as material quality is concerned. Work will proceed in the area of die design in these runs in a continuing effort to improve material quality and study impurity redistribution.

C. Buckle Characterization

Buckle characterization with respect to type, period, and amplitude has been started to obtain baseline data for typical growth conditions encountered with the present design of the 7.5 cm cartridge. A profilometer has been used to trace surface profiles of ribbon grown below 4 cm/min. Traces obtained from runs 18-103 and 18-105 are shown in Figs. 1 and 2. These traces represent typical buckle patterns observed over a speed range from about 2.5 cm/min to 4 cm/min.

Although the interpretation of the patterns is complicated by such factors as variations in ribbon thickness and interference from the ribbon contacting the sides of the cartridge growth slot, several distinct features of the buckle formation are worth pointing out. For the thickest ribbon, which is usually grown at the lower speeds, the predominant buckle pattern is one of alternating edge buckles, as shown in Fig.1. The buckles alternate from one ribbon edge to the other with a

EDGE   CENTER   EDGE
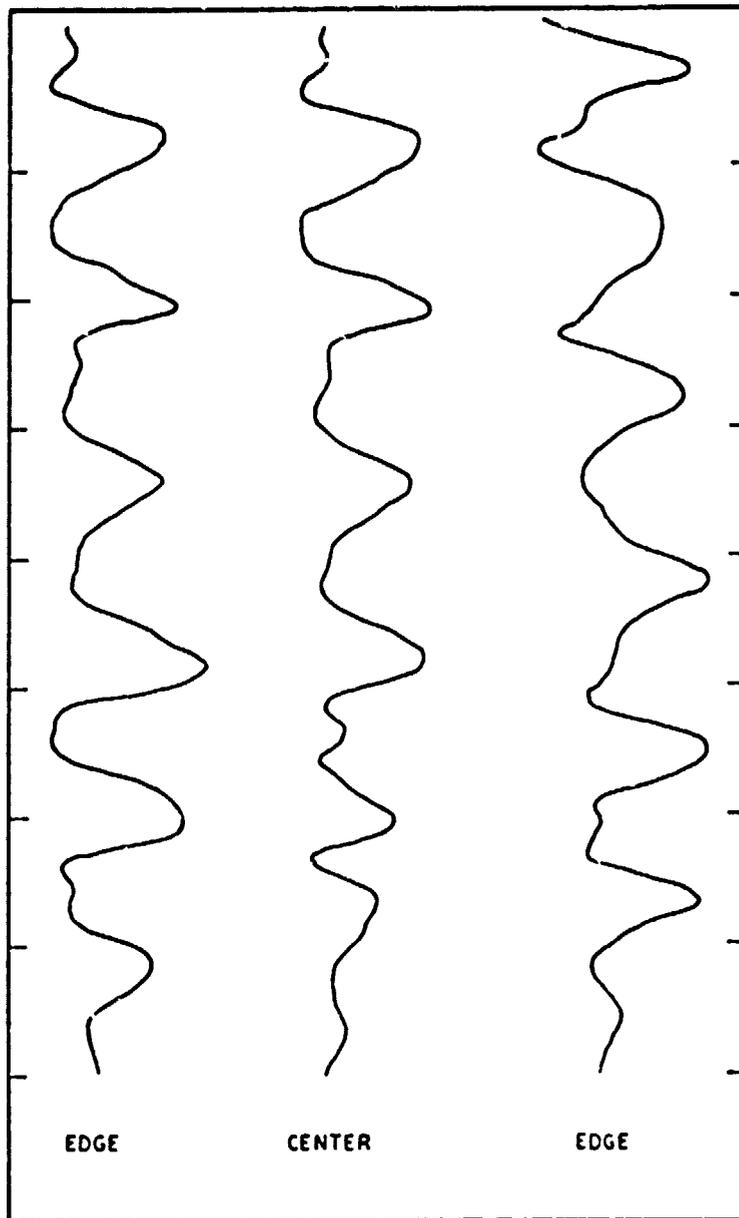
Fig. 1. Surface profile traces illustrating typical edge
buckling for ribbon no. 18-102-2 grown at a speed
of 3.0 cm/min. Traces are taken along the growth
direction, with respect to the width dimension as
marked.
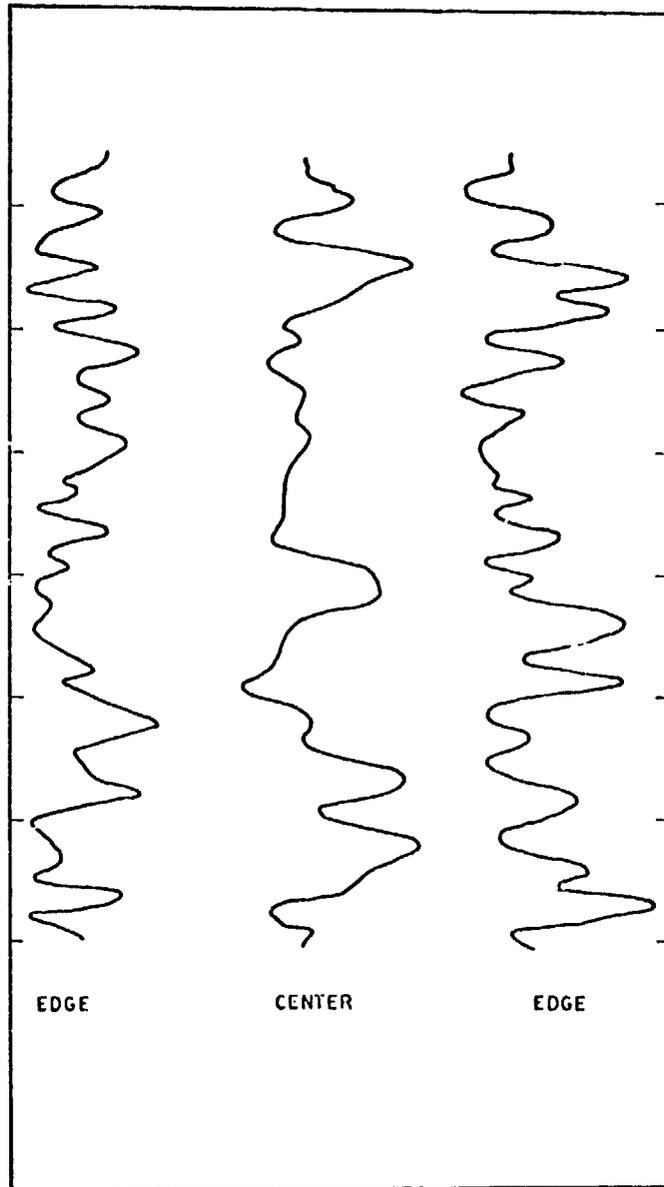
Fig. 2. Surface profile traces illustiating typical center buckling
for ribbon No. 18-105-1 grown at a speed of 3.6 cm/min.
The background modulation may be due to interference from
ribbon guidance system or edge buckling.

period of close to 8 cm, of the order of the ribbon width. Buckle periodicity over longer lengths appears to be perturbed and often destroyed as a result of what is interpreted to be the interference of the ribbon with the cartridge growth slot walls. This slot is about 0.15 cm wide and would act to guide the ribbon if the buckle amplitude were to become great enough to bring the ribbon in contact with the wall. For thinner ribbon, which is usually obtained at higher growth speeds in the present system, the edge buckle pattern appears to give way to ribbon center buckling. This is illustrated in Fig. 2. This shows an intermediate situation where a shorter period buckling, corresponding to the center buckling, is starting to dominate the longer period edge buckling. The period of the center buckles varies from 2 to 3 cm.

III. MULTIPLE RIBBON FURNACE by B. H. Mackintosh

A. Overview

By the end of the third quarter, previous difficulties with severe growth instability and heavy concentration of silicon carbide particles on ribbon surfaces had been reduced by eliminating backstreaming of atmosphere into the furnace. It had also been shown during the second and third quarters that the furnace was approximately as clean as the wide growth furnace no. 1 with regard to metallic impurities. A series of baseline quality runs at the end of the third quarter produced ribbon with light to moderate silicon carbide particle density (~ 1 to 4 per cm^2), tielding cells with average AM1 conversion efficiencies of 6% (AR coated).

At the beginning of the fourth quarter, two additional measures were taken to promote growth with a higher meniscus, which tends to reduce the density of surface carbide particles. The first was to institute a cartridge gas flushing flow which would keep the furnace ambient off the meniscus, and the second was to begin using dies with a wider top slot, i.e., .038 or .05 cm instead of the .025 cm dimension previously employed as standard.

Simultaneously, a set of experiments was begun with saw-cut capillary dies and displaced-tip (asymmetric interface) dies. All 5 cm ribbon growth work through the end of the third quarter had been performed using drilled multicapillary dies. Theoretical work conducted over the past year in this project on fluid flow and distribution of impurities predicted the possible benefits of die capillary configurations which promote lateral flow past the growth interface. The multicapillary die does not effectively create this condition.

I .ad also been demonstrated in the work of furnace no. 1 by the end of the third quarter that improved device parameters resulted when the die was modified to create an asymmetry, through the thickness dir-

13

ection, in the meniscus. Accordingly, these two principles of die design were implemented in the 5 cm cartridge during the fourth quarter. Runs were made with each feature (center saw-cut capillary, and asymmetric interface) separately, and then with both features together.

To furnish information toward resolution of the ongoing question of effects of quartz vs. graphite crucibles, each crucible type was used at least once with each die type. A range of tip displacement dimensions was evaluated in the asymmetric interface die runs.

Experiments of this quarter also included the evaluation of three configurations of end-stabilizing bulbs, which are unique to this system. Here the goal was to find a bulb configuration which would work well in conjunction with tip displacement. As a result of these growth experiments, a die design was chosen for the upcoming multiple growth runs which represents a good compromise, within current knowledge, between stable, reliable growth and enhancement of solar cell performance through impurity distribution.

Fabrication and assembly work on the new multiple hot zone proceeded to the point of readiness for initial heat-up at the end of December. Two views of this unit are shown in Figs. 3 and 4. The overall multiple growth system was out of operation for approximately three weeks in October and November while the five growth stations were outfitted with the improvements to the cartridge temperature control systems described in previous reports. The system will be ready for 5-cartridge operation after the following tasks have been completed:

- Basic testing and longitudinal temperature profile trimming of new hot zone.

- Purification of hot zone components in their final form.

- Assembly of ⌐⌐ graphite trap door system.

- Debugging and calibration of temperature and puller control electronics of remaining four stations.

- Procurement of dies with optimum design features as determined from recent experiments.

B. Details of Growth Activity

Table II lists the runs of this period in numerical order. Solar cells were made from ribbon grown in runs 154 through 160. Due to difficulties in solar cell fabrication, no devices have yet been completed for
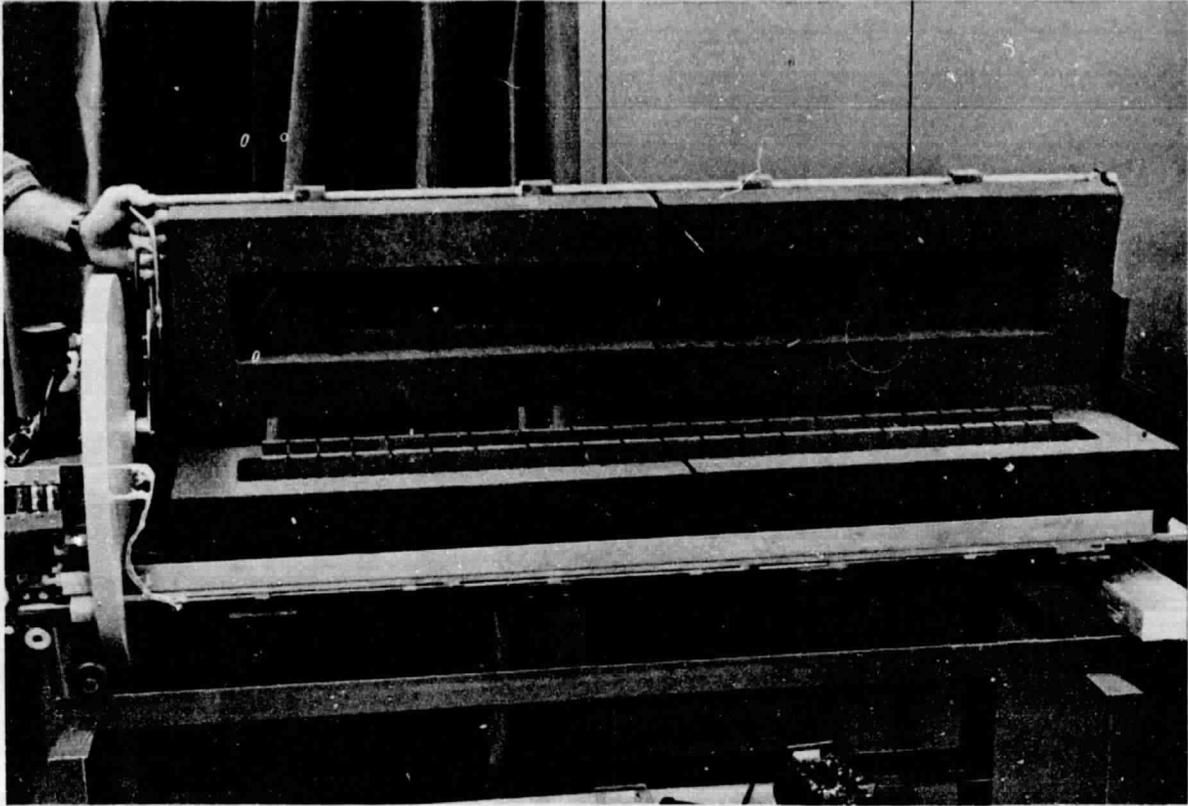
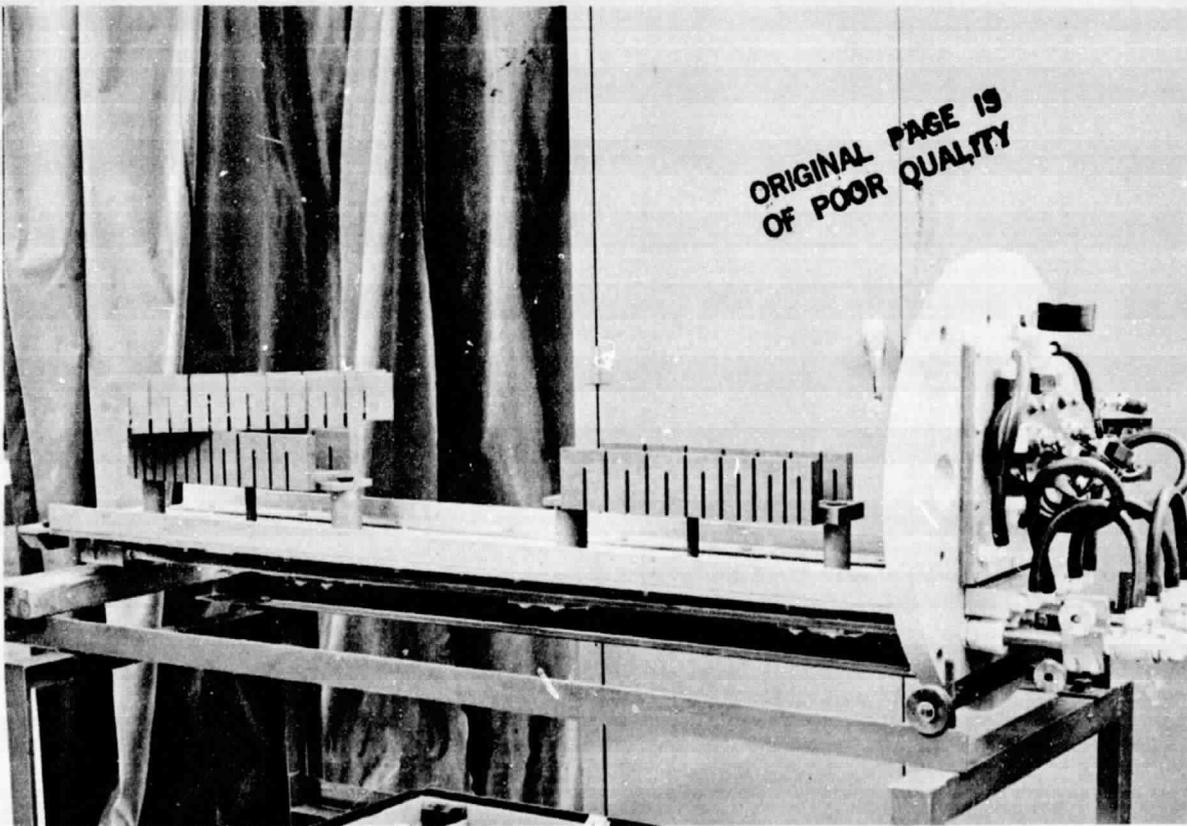Fig. 3.   New hot zone partially assembled.

Fig. 4.   New full length hot zone for furnace 3A.

Run No.	Crucible Type	Die Type·	Length Grown (M)	% Full Width	Comments
154	G	SC .05 slot	4.1	95	Straight bar end heaters and SC capillary result in high central portion of meniscus ribbon center clear of SiC.
155	Q	SC .05 slot	1.7	88	Experiments with cartridge flushing flow - clearly improved stability. SiC density varied widely during run.
156	Q	SC .05 slot	3.0	83	Cartridge flushing used during most of run. Ribbon center clear as in runs 154 and 155 due to high center meniscus.
157	G	SC .05 slot	5.4	87	Changed to wrap around end heaters; flattened meniscus. Free of SiC except narrow strips at edges.
158	G	SC .05 slot	4.1	92	Similar to 157 but slightly higher speed; higher meniscus promoted very low SiC throughout run.
159	G	MC, displ. .038 slot .012 displ.	8.6	50	High meniscus side perfect'y clear. Less stable than with previous thicker, SC capillary die.
160	G	MC, displ. ,038 slot .007 displ.	7.6	60	High meniscus side had light SiC particle concentrations.
161	G	SC, displ. .038 slot .007 displ.	5.1	53	Similar results to 160. First bulbous ended displaced die. Bulbs not as effective as in nondisplaced die.
162	G	SC, displ. .038 slot .012 displ.	4.3	47	Similar results to 159. Growth from bulbs not stable
163	G	SC displ. .038 slot .012 displ.	5.8	31	Similar results to 162. Bulb modified by widening notch. Did not improve stability.
164	G	SC, displ. .038 slot .012 displ.	5.5	0	High side bulb surfaces filed down to same level as low side surfaces. Ribbon edges very unstable.
165	G	SC, displ. .038 slot .007 displ.	6.5	60	End heaters trimmed to locally heat extreme die ends. End stability fair.
166	G	SC, displ. .038 slot .011 displ.	6.0	90	Holes drilled through die ends to feed mel' to bulbs. End stability good. High meniscus side very smooth - no SiC.
167	Q	MC .025 slot	11.2	29	Previous standard MC die with top slot. Flared at ends, as experimental means of edge stabilization. Thin ribbon grown wit! fair stability at ~ 4.1 cm/min but high Si(particle density.
168	Q	SC, displ. .038 slot .012 displ.	4.6	24	Same die modification as in 166. Poor end stability; high meniscus side clear.
169	Q	MC, displ. .038 slot .007 displ.	7.4	0	Test flared ends of top slot with displace ment. Stability poor and growth hindered by SiO deposits blocking view slot on outside of cartridge.
170	Q	SC, displ .038 slot .012 displ.	5.3	33	Main zone (crucible) temperature lowered but did not reduce buildup of SiO on cartridge. Run ended prematurely due to block(view.
171	G	SC, displ. .038 slot .012 displ	5.5	71	Die machined with front and rear bulb flat. at same height as high tip. Also used buli feeding capillaries as in 166. Excellent stability.

Table II. Summary of Furnace 3A Growth Runs, Fourth Quarter

16

runs 161 through 171. The results of each of the three variations from the previous standard die (multicapillary, non-displaced) are discussed in the following sections.

1. Saw-cut Capillary Dies

Because of the requirement for excellent growth stability and long-term die performance reliability in the eventual 5-ribbon operation, a decision was made not to experiment with dies of the drilled center capillary type. Although the best solar cells ever produced by a cartridge-type EFG system were made from drilled center capillary dies, this die type has proven susceptible to interruption of flow due to silicon carbide growth in the capillary holes. Instead, the saw-cut capillary die was chosen as an improvement over the multicapillary die used in previous 5 cm growth work. While the transverse component of flow next to the interface in the saw-cut capillary die is not as great on average as in the drilled center capillary die, the lack of abrupt changes in flow path cross section area near the interface avoids areas of stagnation where, in center capillary dies, silicon carbide preferentially grows. Control of spreading during growth is easier with saw-cut than with multicapillary dies, as the local hot spots caused by hot fluid exiting from the capillaries are absent. A change was made from straight bar end-heaters to wrap around end-heaters, to better match the "warm center" characteristic condition of this die. The combination of wider die top slot (hence thicker ribbon), smooth capillary flow distribution, and the cartridge flushing gas flow instituted at this time resulted in extremely stable growth.

The first four runs (two with graphite crucibles and two with quartz) employing saw-cut capillary dies were performed the last week in September and the first week in October, prior to the issuance of the Annual Report. A summary of solar cell properties from these runs was reported there. Two more graphite crucible runs, number 157 and 158, completed the series using saw-cut, non-displaced ("flat") dies. Solar cell parameters on the four graphite-crucible runs are fairly closely grouped and show a distinct improvement over multicapillary die baseline runs earlier in the year, up to the level of >8% AM1 efficiency (AR coated). Part of this improvement may be ascribed to the further reduced density of silicon carbide particles, down to the range of 1 particle per cm^2 or less. Conclusions about the role of more favorable distribution of im-

17

purities in this material must be based on additional characterization work.

Growth conditions were similar in the two quartz crucible runs; silicon carbide was once again light. Solar cell parameters for both runs are slightly higher than the values for the preceding and following graphite crucible growth. The slight differences and the small data base do not yet warrant conclusions.

2. Asymmetric Interface Dies

Three runs were conducted using multicapillary dies modified simply by machining one flat to .007 or .012 cm lower than the other, and widening the transverse top slot from .025 to .038 cm. Solar cells were made from the first two runs, which were from graphite crucibles (Table VI). The differences in cell parameters probably reflect different degrees of asymmetry induced by the two displacement dimensions used in these runs (refer to Table II). The larger dimension in the die of run 159 resulted in ribbon with one side perfectly clear of silicon carbide particles, whereas the opposite face was decorated with an extremely high density (10 per cm^2) of small particles. With the smaller dimension run 160, these surface characteristics were not so extreme; a few particles were present on the high-meniscus side. It is assumed that the deposition on one face of the ribbon of all or most of the silicon carbide is one mechanism of improvement of photovoltaic properties, but not the sole mechanism.

Other mechanisms by which an asymmetry in the thermal and geometric conditions of the growth interface may affect device performance, and measurements made to assess these mechanisms, are discussed in section V of this report and in the 1978 Annual Report.

3. Displaced-tip, Saw-Cut Capillary Dies

These six runs reproduced the results of the two runs discussed in section 2 above, insofar as a tip displacement of .012 cm consistently resulted in growth of ribbon with one side perfectly clear of SiC, while a displacement of .007 cm resulted in reduction but not elimination of SiC from one face. As the most efficient solar cells to date resulted from runs in furnace 1 employing displaced, center capillary dies, it is assumed that some of the displaced, saw-cut dies runs (nos. 161, 162, 163, 164, 165, 166, 168, 170, and 171) will also produce the best cells in this overall group. The only property measurements made to date on this

material, SPV L_D, show unprecedented high values, both peak and average, for several of these runs. Of particular interest are runs 166 and 171. In both cases, the relatively large die displacement yielded ribbon with the high-meniscus side clear, while growth conditions were stable and several meter lengths of full width ribbon were grown without any operator adjustment. The series of end-bulb modifications described in table II culminated in the die of run 171 which displayed excellent long-term stability. A similar die, with .041 cm top slot, .011 to .014 cm displacement, a saw-cut capillary, and bulbs with both front and rear halves at the same height as the high side tip, is being made in quantity for the upcoming multiple demonstration runs. Ribbon approximately .038 cm thick will be grown at 3.5 cm/min. At this combination of thickness and growth rate, the ribbon will be essentially flat, as required to facilitate processing of the large number of cell blanks which will result from these runs.

C. Future Work

After the capability of furnace 3A to produce 5 cm ribbons, five at a time, with quality suitable for a 70% yield of 9% AM1 efficient devices, has been demonstrated, work with 5 cm ribbon will end. In the coming year, furnace 3A will be the first system to be converted for development of 10 cm wide growth. Design of a basic 10 cm cartridge is underway. The first phase of growth activity with this unit will begin around mid-March, while furnaces 1 and 17 carry on their respective programs of work with 7.5 cm ribbons. A new theory of buckle generation currently under discussion at Mobil Tyco will enter into design of the cold shoe/afterheater components of the new cartridge; some of the experiments planned for system 17 will attempt to verify and extend this theory. One of the goals for the year of the overall project is a reliable cartridge with throughput rate of 10 cm width at 5.6 cm per minute. It is hoped that the work performed in the coming year with furnace 1 will provide the understanding of how to maintain or surpass the level of solar cell efficiency thus far demonstrated (9 to 10%) in ribbon growth at this substantially greater speed.

IV. MACHINE 17 by E. Sachs

A. Overall Objectives

This was the first full quarter of operation for machine 17. The primary goal for this quarter was to attain stable, full width, repeatable growth. It was felt that the attainment of such conditions was a prerequisite for all experimental investigations which are to follow. As is described below, this condition has been attained.

However, work was also accomplished along other lines. A good deal of effort was successfully invested in the development of video processing techniques for the attainment of edge position and meniscus height information directly from the video image as presented by the anamorphic optical-video system. This information can provide the basis for closed loop control of cartridge die heaters.

Attention was also directed at the question of ribbon flatness and stress. As thermally induced stresses and buckling will be the first main thrust of experimental investigation on machine 17, we felt it imperative to strive toward a high degree of separation of the problems of thermally induced buckles, and guidance induced ripples. As such we have taken measures that allow us to grow ribbon that is fairly free of guidance induced undulations. The attainment of stable, full-width growth has also allowed us to begin the task of developing a tool with which to measure residual stress levels in grown ribbon. Without such a tool, efforts at stress minimization will be greatly hampered.

B. Video Processing

The first step, and often the most difficult one, in building an automatic control system is the acquisition of the relevant information from the system being controlled. In ribbon growth, the geometry of the growing ribbon is determined by edge positions and meniscus height.

Figure 5 illustrates a method for obtaining this information from
the video image as seen by the anamorphic optical-video system. Figure
5(a) is the normal image as seen through the optical-video system. A de-
vice called a video quantizer is then used to create the purely black
and white image seen in Figs. 5(b) and 5(c). This device allows one to set a
video threshold value. Any picture point above this threshold in in-
tensity is turned totally white, any point below it is turned black, thus
maximizing the image contrasts. Figure 5(b) shows the threshold value ad-
justed to delineate the ribbon edges while in Fig.5(c), it is adjusted to
delineate meniscus height. The final piece of video analysis hardware
is a video integrator, a device which superimposes on the screen a win-
dow of variable height, width, and position. The integrator then gives
an analogue signal proportional to the average of the video intensity
falling within the box. With an image that is quantized (fully black-
white) this average is a linear indicator of the position of an edge
position on the meniscus height. Figure 5(b) shows the integrator box ad-
justed to pick up an edge, while Fig.5(c) shows it on meniscus height.

These two pieces of video analysis equipment are off-the-shelf hard-
ware from Colorado Video, Inc., Boulder, Colorado.

It has been found that this technique is capable of resolution of
edge position to within ±.002 cm, limited apparently by the grain of the
TV camera tube. The meniscus height resolution of the optical video sys-
tem at any given point is on the order of .001 - .002 cm limited by both
optical and TV imaging resolution. However, because the video integra-
tor box extends over a substantial portion of ribbon (1 cm or more), it
is in fact supplying a spatial average of meniscus height. As such, TV
camera grain is spatially averaged resulting in resolution of average
meniscus height that is considerably better than .001 cm. In fact, .002
cm amplitude meniscus fluctuations due to periodic puller speed varia-
tions are detectable with excellent resolution. The only problem en-
countered to date with this video analysis technique is that of long term
drift. While it does not affect meniscus height measurement, this drift
does reduce the overall accuracy of the edge position measurement to
approximately ±.010 cm.

The precise cause of this drift remains uncertain; however one prob-
able cause is as follows: with the video analysis system described above,
the edge position is measured with respect to a reference point in the
TV signals (the horizontal line synch pulses). Thus, if the TV tube de-

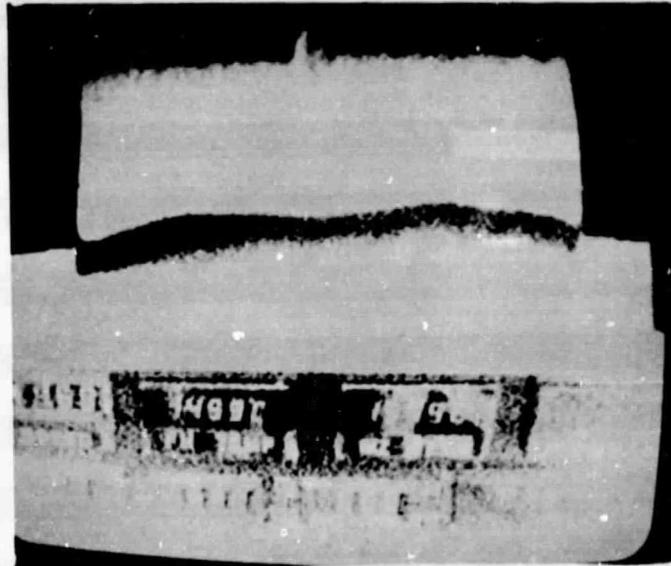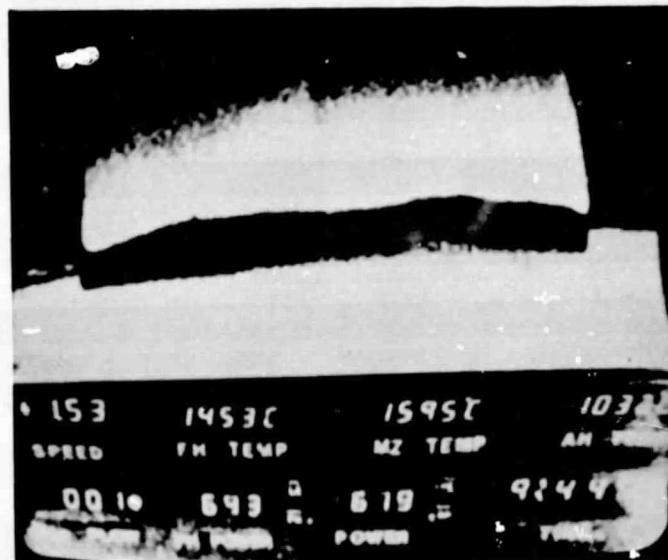(a) Full grey scale image from TV screen

ribbon

meniscus

die

(b) High contrast image with video-integrator on ribbon edge

video analysis box

(c) High contrast image with video-integrator on meniscus height

video analysis box

Fig. 5.   Video Analysis

23

flection voltage (or any of a long list of parameters) changes, it will change the measured edge position. This type of drift may be corrected by simultaneously measuring the position of the ribbon and the die edge near it, and subtracting the two signals. The result will be a signal proportional to the distance between the ribbon edge and the end of the die, and, as fluctuations in line voltage, etc. will contribute to the two signals, the resultant position signal will be insensitive to many of the factors that may contribute to the drift now observed.

C. Growth Runs and Results

During this quarter, nine growth runs were made. The progress made on these runs, and the experimental results obtained are described below. All growth runs were with a cartridge with no cold shoe. The cold shoe was removed for several reasons, as described in the previous quarterly report. The primary reason was to simplify the thermal environment seen by the growing ribbon. Once simplified and made highly reproducible, reliable and understandable correlation between measured temperature profiles and thermal stresses can be undertaken.

1. Progress in Growth

The first runs were really shakedown runs in which we became more familiar with the equipment. Generally, about 3 m of ribbon were grown in each run, ranging in width between 2 and 7 cm. Although several lengths of almost full-width ribbon were grown, growth was not reliable. Gradually our performance increased over the course of the runs conducted with the result that the last four runs resulted in almost entirely full-width ribbon, with long intervals between freezes (in some cases, more than one hour). One such ribbon is shown in Fig. 6. In three of the last four runs the crucible was emptied.

In the last of the nine runs we purposely grew ribbon with a low afterheater setting resulting in high residual stress. This ribbon was used to evaluate various stress measurement techniques described later.

The marked improvement in our ability to grow ribbon can be attributed to three factors:

1. Familiarity with the system
2. Adoption of full width seeding techniques
3. Use of a die with a certain amount of built-in thermal/capillary edge stability. In the last four runs of this quarter bulbous dies were used
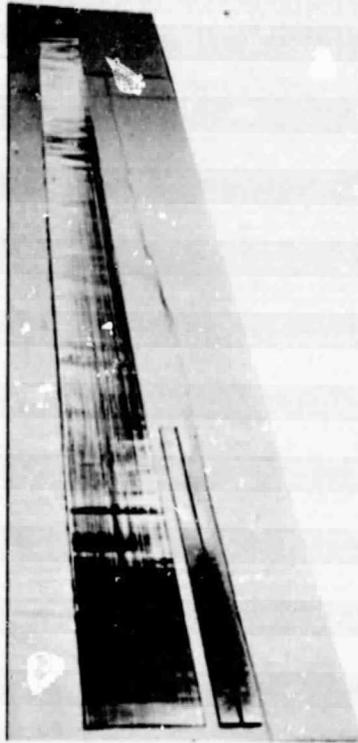
Fig. 6. A full width, bulbous ended ribbon. A 1 foot
rule is shown at the right.

which resulted in the growth of ribbon with
bulbs of approximately circular cross section
of a diameter approximately twice the ribbon
thickness.

We may now confidently say that our future experimentation will be
facilitated by our ability to grow stable, full-width ribbon.

2. Ribbon Flatness-Guidance

In order to separate the problems of thermal stress and buck-
ling and guidance induced ripples, attention has been paid to proper
alignment and guidance in the growth system. Two basic changes have been
made:

1. Ribbon guidance has been improved.

2. We have adopted the procedure of carefully check-
   ing the alignment of the puller axis and the die
   prior to each run.

The result has been a marked improvement in the ribbon. It is
believed that further refinement of the guidance is still possible.
In any event, the current level of guidance induced ripples is suffi-
ciently low to allow an investigation of thermal stress to proceed.

3. Silicon-Carbon Ribbon Thermocouples

A ribbon thermocouple trace was taken in a cartridge without a
cold shoe so as to refine the technique used in acquiring this data and
begin a catalog of the temperature profiles seen by the ribbon for the
thermal stress experiments.

The dotted line in Fig. 7 presents the results of a temperature
profile taken with a standard W-Re thermocouple in the center of the
afterheater. A tracing was also made down the side of the afterheater,
with the same thermocouple showing a 25°C lower reading than the central
trace for the first 4 cm from the die and converging thereafter.

The solid line represents a temperature profile taken with a sili-
con carbon ribbon thermocouple in the center of the ribbon. Note that
this trace gives a much more reasonable looking profile in the region
near the die than does the conventional thermocuple.

Fig. 7. Temperature profiles of run 17-011. The dotted line is a
profile taken with a W-Re thermocouple. The solid line is
the result of a silicon-carbon thermocouple trace.

As it is this region of higher curvature that is of interest from the point of view of thermal stresses, it is imperative to obtain this information by the use of the ribbon thermocouple technique.

The last data point obtained was .2 cm from the interface. As such, it is difficult to infer with precision the temperature gr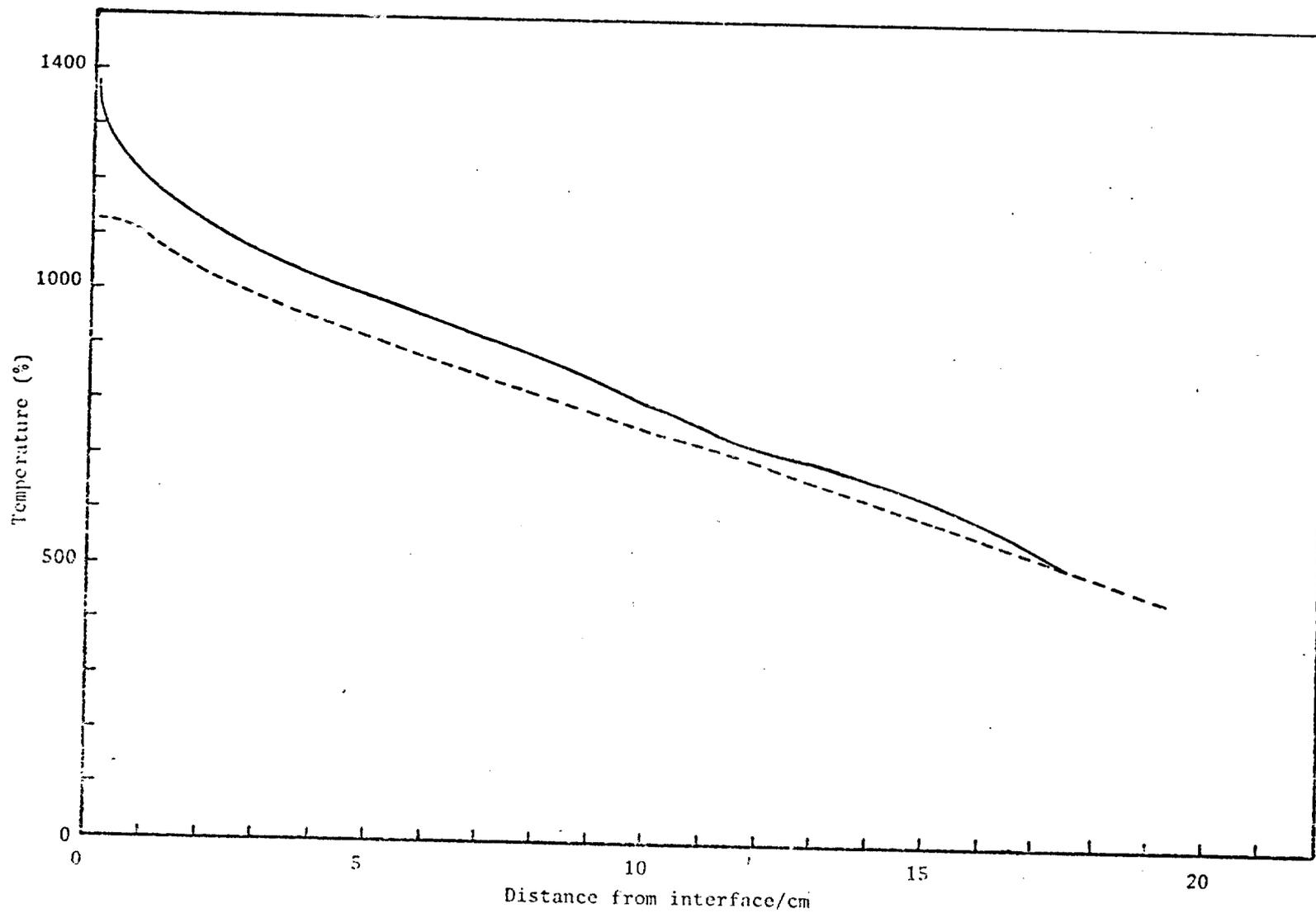adient at the interface, as the data may be extrapolated to yield anything between 800°C/cm and 1500°C/cm. However, it is of interest to note that this range of gradient would infer a maximum growth speed between 2.3 cm/min or 4.3 cm/min, for the thickness of ribbon used to profile the system. The observed maximum growth speed is approximately 2.5 cm/min, thus lending credence to the measurements.

This data was taken by recording it on video tape as the melt-in proceeded. Hence, the amount of data available is limited only by the resolution of the displacement transducer on the belt puller. In addition, video tape recording of the data allows the experiments to concentrate fully on other aspects of the measurements.

D.   Thermal Stresses

As mentioned, the first concentration of investigative effort on machine 17 will be in the area of thermally induced stress and buckling. The first series of experiments will be carried out in a cartridge without a cold shoe. As explained previously, the simple thermal system resulting from the removal of the cold shoe will represent an understandable and repeatable starting point for the examination of thermal stresses. It is planned to correlate the state of stress of grown ribbon with detailed horizontal and vertical temperature profiles as measured by silicon-carbon ribbon thermocouple traces. Modifications of these temperature profiles will be effected and assessed by the change in the state of stress in the grown ribbon. As such, it is imperative to have a technique by which to assess the state of stress of a ribbon. Several techniques have been used and are being investigated.

Several samples of ribbon have been sent to Photoelastic Company to evaluate the potential of infrared photoelasticity. Wire resistance strain gages have been evaluated for residual stress measurement and found to be of insufficient resolution. The technique used was to cement the gage to the whole ribbon, take readings, scribe and break the ribbon around the gage and take readings again. Since the gages used were quite small (½ cm on a side), it was hoped that the small piece of ribbon under a broken out gage would relax to zero stress levels, and the difference

between gage readings would provide a measure of residual stress levels in the whole ribbon. However, the low strain levels in even our highly stressed ribbon (approximately 2×10^{-4}) were not sufficient to bring the signal out of the noise caused by ambient temperature changes and other such factors.

We have also begun investigating the use of the piezoresistive effect of the silicon itself as an indicator of the stress level. This may be thought of as making use of the ribbon as an in situ semiconductor strain gage. The principal concern here is that the change in resistance upon application (or relief) of stress may be found to be too sensitive to crystallographic orientation and structure.

In the next month we will try what is perhaps the most promising technique. A ribbon will be fastened to a substrate and sawn almost its full length in ten even spacings across the width. The ribbon will then be released and the displacements of each of the ten or so fingers from its initial position will be measured. This will essentially provide a measure of the stress gradient in each finger from which the complete stress distribution across the width may be determined. In essence, this technique will be a refinement of the commonly used scribe and split technique which will permit greater resolution of stress gradients across the width.

V. MATERIAL AND CELL CHARACTERIZATION

A. Material Characterization by J. F. Long

A routine run-by-run material characterization program has recently
been mapped out. Material type and resistivity will be determined by the
four-point probe method. The resistivity will be verified, while majori-
ty carrier mobility and concentration will be determined by the Hall/Van
der Pauw technique. Schottky barriers will be fabricated for the mea-
surement of the minority carrier diffusion length via the SPV method, and
for infrared scan measurements. To this end, special evaporation masks
have been designed and fabricated. Additionally, other available elec-
tronic and optical characterization techniques will be employed where
specific growth experiments warrant them. Figure 8 is a flow chart ill-
ustrating the manner in which the material will be handled.

1. Furnace No. 1

Material from displaced die runs has been selected in order to
study the differences between the high and low meniscus sides. A distinct
difference in the appearance of the two surfaces has been noted. The "B"
or low meniscus surface very often possesses high SiC particle densities
and is always rough in appearance, while the "A" or high meniscus surface
is always smooth and SiC free. Studies of the minority carrier diffusion
length for each of the two surfaces have thus far been inconclusive. Al-
though the average diffusion length for measurements on the "A" side has
thus far always been higher than for the "B" surface of the same sample,
the difference is not always large. Further, questions have arisen re-
garding the accuracy of the diffusion length extrapolation involved in the
SPV data reduction process for short diffusion length material. These
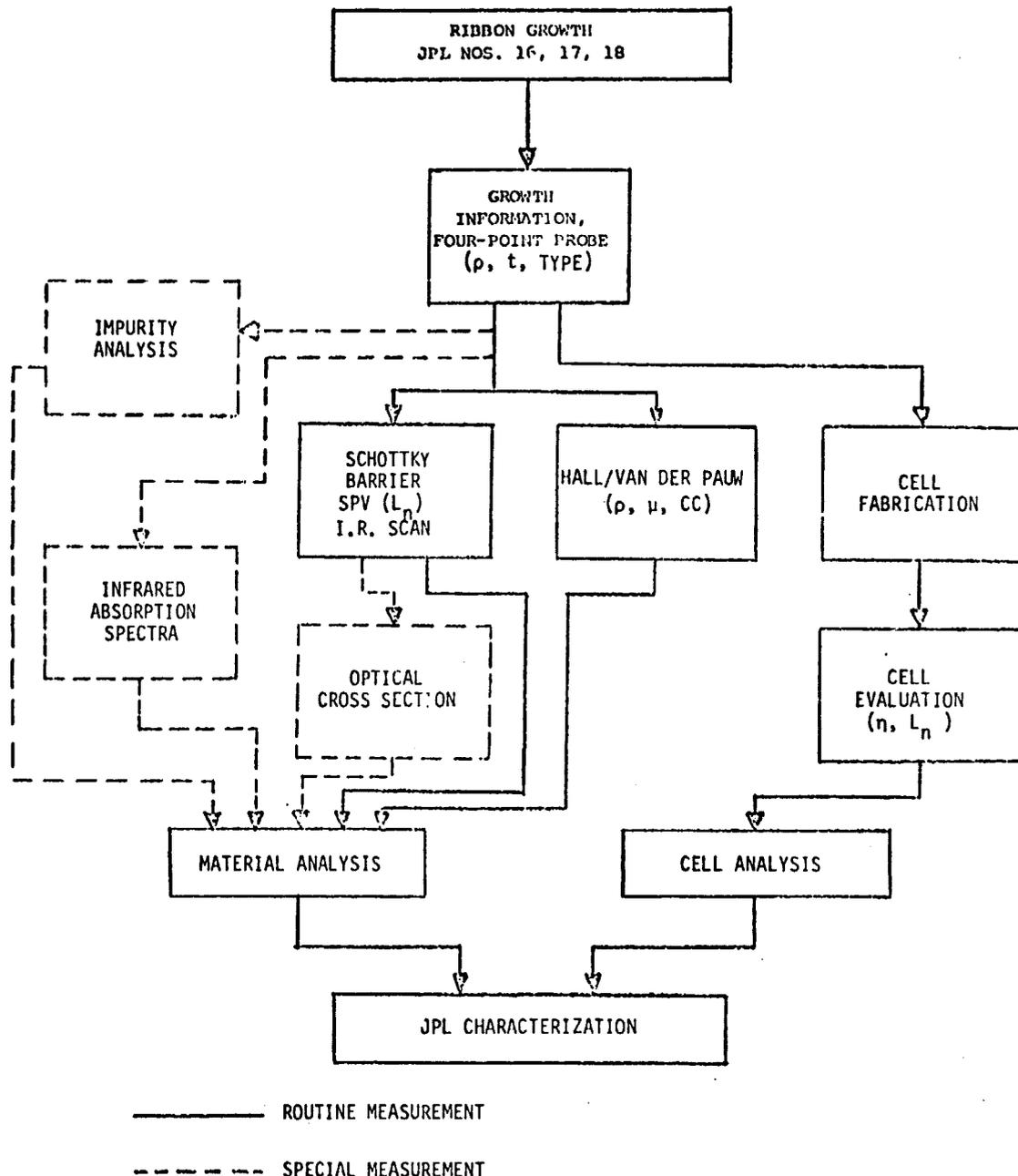questions are currently being examined.

Fig. 8.   Flow Chart for Material Characterization.

2. **Furnace No. 3A**

The aforementioned characterization program was implemented for a series of runs from 16-155 through 16-170. Various combinations of crucible and die type were utilized for these runs. Particular attention was paid to die design, with a number of modifications made in attempts to improve both growth stability and electronic quality[2]. All the runs were nominally doped to 1 Ω-cm; run averages for resistivity via four-point probe were 1.1 - 1.4 Ω-cm. Van der Pauw resistivity ranged from 1.0 to 1.9 Ω-cm; majority carrier mobility and concentration ranged from 132 to 248 cm^2/V-sec and from 2.2 to 3.2 x 10^{16}/cm^3, respectively. Because of the questions about the SPV data reduction already mentioned, interpretation of the diffusion length averages is difficult, but it does appear that the displaced die grown material exhibits somewhat higher diffusion lengths. More data will be taken, and the questions about the data reduction will be addressed. Infrared (1 μm) photocurrent scans on the material from these runs are still being done; thus far, the spatial current inhomogeneity typical of resistance grown material is evidenced for all of the die/crucible combinations. More data will be gathered before any attempt is made to correlate gross spacial trends with predicted fluid flow impurity redistribution patterns.

B. **Cell Characterization** by C. T. Ho

Routine solar cell evaluation for various crucible type, die configuration, is being continued. The "state-of-the-art" photovoltaic conversion efficiency for cells fabricated from ribbons grown from system no. 1 was found to be 9.1 - 9.4% with the cell size 17-18 cm^2, and 8.4 - 8.8% with the cell size 54-58 cm^2. In both cases the highest achieved cell efficiency is ~ 10%.

1. **Growth Station No. 1 - Wide Ribbon Growth Furnace**

a. **Repeat of the Optimum Run, No. 18-102**

In the last quarter, we have reported that the growth run no. 18-102 in which a graphite crucible and a central capillary displaced die were used, produced an average optimum photovoltaic conversion efficiency of 9.35%. A following growth run no. 18-103 was cut into 7 x 2.3 cm^2 cell blanks, and a photovoltaic junction was formed on the SiC-free surface. The solar cell outputs under a 100 mW/cm^2 ELH light intensity are shown in Table III. The results in the table clearly indicate that it has reproduced the optimum photovoltaic quality. These two runs represent the "state-of-the-art" result for the material grown from the furnace.

33

Table III. Solar Cell Data for Ribbon Material Grown from Run 18-103. Cells are 2.5 x 7.5 cm^2, cut across the ribbon width.

100 mW/cm^2, ELH light, 28°C, AR coated

Cell No.	I_{sc} (mA/cm^2)	V_{oc} (V)	FF	P (mW/cm^2)
1031	25.78	0.539	0.663	9.22
1032	25.30	0.544	0.668	9.20
1033	24.45	0.532	0.672	8.74
1034	24.89	0.535	0.656	8.73
1035	24.50	0.532	0.670	8.73
1036	24.88	0.541	0.671	9.03
1037	25.13	0.538	0.636	8.60
1038	26.64	0.546	0.653	9.50
1039	26.57	0.550	0.685	10.02
10310	24.66	0.544	0.697	9.36
Mean Value	25.28	0.540	0.667	9.11
Standard Error	0.254	0.0019	0.0054	0.139

Table IV. Large Area (~ 7.5 x 7.5 cm^2) Solar Cell Data for Ribbon Materials Grown from the Optimum Runs 18-102 and 18-103.

100 mW/cm^2, ELH light, 28°C, AR coated

Run No.	Cell No.	Area (cm^2)	J_{sc} (mA/cm^2)	V_{oc} (volt)	FF	η (%)
18-102	L-102-1	53.6	24.29	.538	.686	8.97
	-2	56.2	22.92	.536	.726	8.92
	-3	54.7	23.22	.528	.695	8.52
	-4	55.0	23.38	.538	.681	8.57
	-5	55.1	22.87	.530	.637	7.72
	-6	55.5	22.59	.530	.638	7.64
	-7	54.3	24.29	.535	.688	8.94
	-8	55.8	23.62	.542	.626	8.03
	Average		23.40	.535	.672	8.41
18-103	L-103-1	56.0	22.95	.538	.707	8.73
	-2	58.5	22.56	.538	.716	8.69
	-3	53.3	22.85	.534	.646	7.88
	-4	54.7	22.98	.533	.728	8.92
	-5	54.7	24.70	.546	.737	9.90
	-6	54.7	24.10	.539	.687	8.92
	-7	54.7	22.67	.534	.730	8.84
	Average		23.26	.537	.707	8.84

Encouraged by the results, we have selected materials from both runs and processed them into solar cells of size 7.5 x 7.5 cm^2. The measurement results (see Table IV) show that more than half of the finished cells have conversion efficiency close to 9%. Notice that one cell (L-103-5) with an area 54.7 cm^2 even achieved an efficiency of 9.9%.

2. Quartz Crucible Experiment

Two growth runs have been made by using quartz crucibles. In run 18-105 a central capillary, regular flat die configuration was used, while in run 18-106 a central capillary die with a .13 mm displacement was employed. Solar cell blanks were cut mostly along the full grown width (7.5 cm for 18-105 and 7.0 cm for 18-106) and a 2.5 cm along the ribbon growth direction, except for several samples in run 18-105. In the latter case, a 2.5 x 10 cm^2 size was cut with the 10 cm length along the growth direction. The solar cell data are tabulated in Table V .

For the 17 to 18 cm^2 solar cells, the photovoltaic quality of the ribbon material grown from these quartz crucible runs is nearly identical regardless of the die configurations used. The overall cell efficiency is lower than that of the cells fabricated from the previous two optimum growth runs. The larger area cells in run 18-105 show better cell characteristics on the average. It is possible that these cells were cut from the higher diffusion length portion of the ribbon which might lead to better average cell performance, since we have shown previously that the variation of diffusion length often exhibits "U" shaped changes across the ribbon width dimension.

3. Diffusion Length Results

From growth runs 18-76 through 18-106, we have selected three to four representative cell samples in each run and made diffusion length measurements by infrared photocurrent response method. The results are summarized in Fig. 9. In the same figure we also list the crucible (graphite or quartz) as well as the die configuration (flat or displaced, capillary feed) used during the growth run. The measured diffusion lengths are between 10 and 33 μm, and show no discernible differences in terms of crucible type and die configuration between the runs.

C. Growth Station No 3A - Multiple Growth Furnace

1. Solar Cell Results

During the quarter, materials from four growth runs, no.16-157 through 16-160 were made into solar cells for quality evaluation. These

Table V. Solar Cell Data for Ribbon Material Grown from
Runs 18-105 and 18-106.

100 mW/cm^2; ELH Light; 28°C; No AR Coating

Run No.	Cell No.	Area (cm^2)	J_{sc} (mA/cm^2)	V_{oc} (V)	FF	η (%)	Notes
18-105 Quartz crucible, central capillary, flat die.	1051	16.65	16.69	0.514	0.679	5.82	Cell length perpendicular to the ribbon growth direction.
	1052	16.79	15.87	0.510	0.658	5.33	
	1053	17.25	16.62	0.520	0.659	5.69	
	1054	17.56	16.12	0.505	0.640	5.21	
	1055	16.90	16.55	0.514	0.660	5.61	
	1056	18.30	17.15	0.515	0.611	5.39	
	1057	18.30	16.72	0.517	0.675	5.83	
	1058	11.68	16.93	0.525	0.695	6.20	
	1059	18.06	16.69	0.513	0.679	5.81	
	10510	18.24	16.92	0.510	0.635	5.48	
	10511	15.25	16.55	0.514	0.653	5.56	
	10515	18.20	16.60	0.527	0.666	5.82	
	Average:		16.62	0.515	0.659	5.65 (8.19)*	
	10512	25.40	17.30	0.521	0.643	5.80	Cell length parallel to to the ribbon growth direction.
	10513	21.41	17.84	0.526	0.704	6.60	
	10514	20.43	18.50	0.529	0.708	6.96	
	Average:		17.91	0.525	0.685	6.45 (9.36)*	
18-106 Quartz crucible, central capillary, displaced die.	1061	16.09	16.93	0.521	0.711	6.27	Cell length perpendicular to the ribbon growth direction.
	1062	16.07	16.20	0.517	0.696	5.83	
	1063	16.94	16.61	0.525	0.718	6.27	
	1064	17.22	16.34	0.519	0.714	6.06	
	1065	16.32	16.53	0.520	0.709	6.10	
	1066	17.23	16.65	0.519	0.678	5.86	
	1067	17.63	16.81	0.523	0.690	6.07	
	1068	17.65	16.82	0.523	0.687	6.05	
	1069	17.34	16.82	0.529	0.717	6.38	
	10610	17.70	16.68	0.520	0.702	6.10	
	10611	17.72	16.91	0.520	0.717	6.30	
	10612	15.79	16.16	0.511	0.609	5.03	
	10613	17.75	15.31	0.507	0.674	5.23	
	10614	17.76	15.59	0.511	0.651	5.19	
	10615	17.84	15.42	0.502	0.675	5.23	
	10616	17.75	15.38	0.504	0.676	5.24	
	10617	17.81	15.71	0.511	0.680	5.47	
	Average:		16.29	0.517	0.688	5.80 (8.41)*	

* Numbers in parentheses are projected values assuming 45% power gain on AR coating.
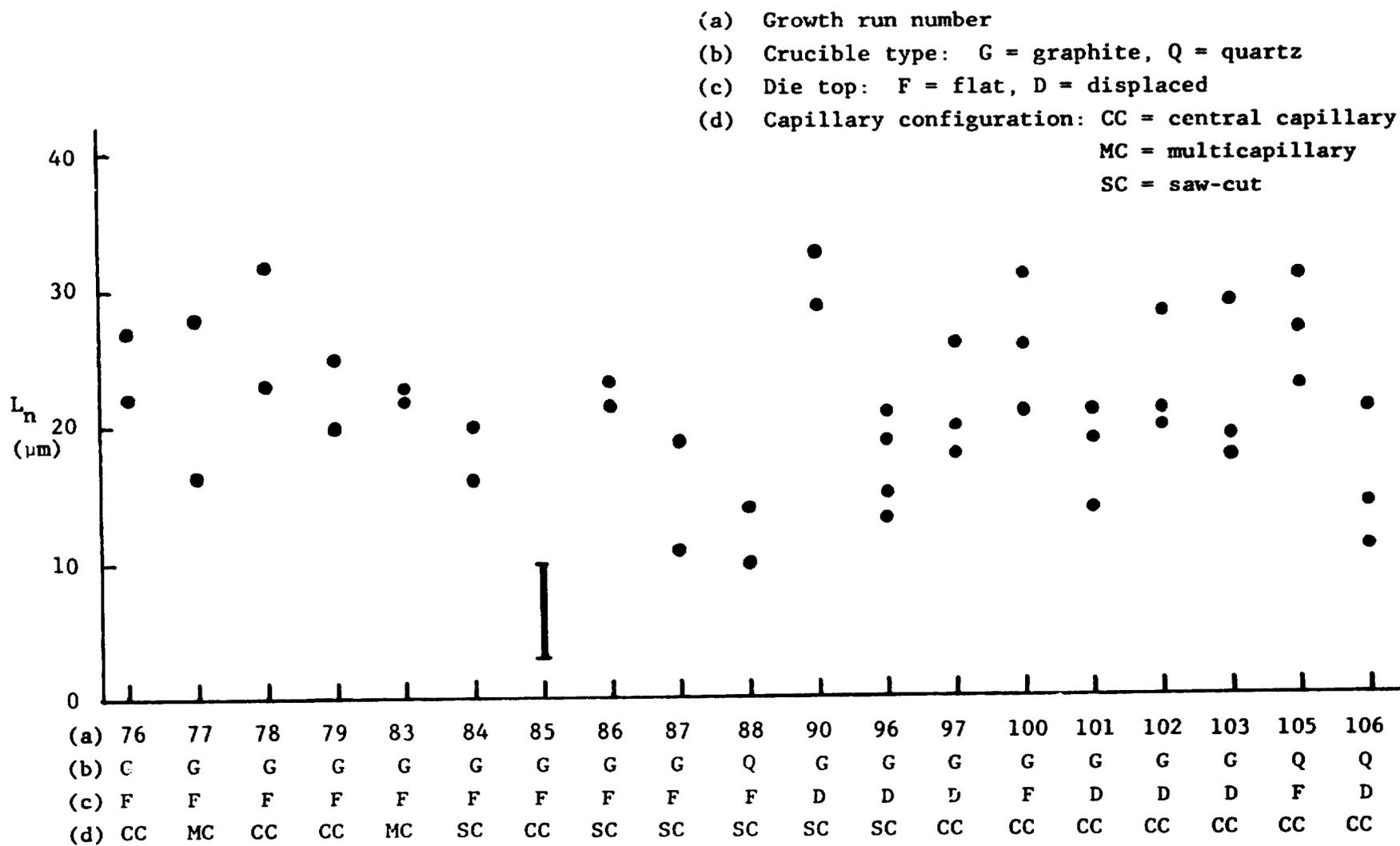
36

Fig. 9. Summary of diffusion length data for ribbon material grown from furnace no. 1.

were all grown by using graphite crucibles. In runs 157 and 158 central saw cut and flat dies were used, while multicapillary and displaced dies were used in runs 159 and 160. The cell outputs are tabulated in Table VI .

The first two runs reproduce the previously established baseline runs such as 16-153 and -154. In the third run, the material yields the same photovoltaic quality in spite of the differences in die configurations. In the last run, the cell output showed slight deterioration. It is possible that the photovoltaic properties are limited by the existence of high lifetime-controlled impurity concentration, which in turn masked the geometric effect of the die on the macroscopic scale.

2. Diffusion Length Results

Diffusion length data has been gathered for the cells fabricated from ten growth runs. The results are summarized in Fig. 10 . Runs 16-135, -144, and -146 were the earlier developmental growths with graphite crucibles, multicapillary dies. Runs 16-154, -157, and -158 were the baseline runs with graphite crucibles, central saw cut dies. The latter run group shows a marginal improvement in the measured diffusion lengths.

The final comparison will be from either the two quartz crucible runs, 16-155, and -156 (with standard flat, saw cut die), or the two graphite crucible runs, 16-159 and -160 (with displaced, multicapillary die) with the baseline run group. The results show that they have similar magnitude varying between 12 - 23 μm but without a clear difference among them.

D.   General Comments   by F. V. Wald

One of the problems in the measurement of electronic properties of the ribbons produced in this program lies in the fact that the properties both over the width and through the thickness of these ribbons are not uniform. Indeed it is a particular aim in the displaced die experiments to increase the inhomogeneity of the ribbon in such a way that the purity and perfection of that side of the material where the junction resides is enhanced and thus better solar cells are produced.

On the other hand, most of the methods used for the numerical evaluation of various ribbon properties, including Hall effect and surface photovoltage measurements, rely on the implicit assumption that properties are uniform in the volumes measured. If that condition is not fulfilled, such measurements may conceivably be subject to several numerical errors

Table VI. Solar Cell Data for Ribbon Materials Grown from Runs 16-157, -158, -159, and -160.

100 mW/cm^2, ELH Light, 28°C, No AR Coating

Run No.	Cell No.	I_{sc} (mA/cm^2)	V_{oc} (V)	FF	P (mW/cm^2)
Run 16-157 Graphite crucible S.C., Flat Die	1571	16.39	0.495	0.611	4.95
	1572	17.89	0.509	0.655	5.96
	1573	17.44	0.510	0.659	5.87
	1574	17.60	0.510	0.639	5.74
	1575	17.22	0.516	0.701	6.23
	1576	17.11	0.504	0.671	5.78
	1577	17.36	0.507	0.640	5.64
	1578	17.24	0.504	0.651	5.66
	1579	16.75	0.506	0.671	5.68
	15710	16.89	0.505	0.708	6.04
	15711	15.58	0.506	0.717	5.66
	15712	17.14	0.508	0.718	6.26
	15713	16.08	0.492	0.649	5.13
	15714	16.18	0.510	0.707	5.83
	15715	16.15	0.506	0.662	5.40
	15716	16.70	0.504	0.698	5.88
	15717	16.71	0.507	0.695	5.89
	Average	16.85	0.506	0.674	5.74 (8.32)*
Run 16-158 Graphite crucible S.C., Flat Die	1581	16.01	0.497	0.539	4.29
	1582	16.21	0.499	0.610	4.93
	1583	17.04	0.505	0.616	5.30
	1584	16.52	0.511	0.649	5.48
	1585	15.55	0.486	0.652	4.92
	1586	16.41	0.506	0.676	5.61
	1587	16.92	0.510	0.677	5.85
	1588	16.76	0.523	0.714	6.26
	1589	16.33	0.508	0.669	5.54
	15810	17.56	0.512	0.679	6.11
	15811	17.00	0.505	0.633	5.44
	15812	16.92	0.517	0.698	6.11
	15813	17.68	0.526	0.718	6.67
	15814	17.19	0.518	0.735	6.55
	15815	16.71	0.512	0.645	5.51
	Average	16.72	0.509	0.661	5.64 (8.18)*

* Numbers in parentheses are the projected values assuming 45% power gain on AR coating.

39

Table VI (Continued)

Run No.	Cell No.	I_{sc} (mA/cm^2)	V_{oc} (V)	FF	P (mW/cm^2)
Run 16-159 Graphite crucible M.C. Displaced Die	1591	17.08	0.516	0.681	6.02
	1592	16.66	0.511	0.678	5.77
	1593	16.12	0.515	0.703	5.83
	1594	16.60	0.516	0.685	5.87
	1595	17.26	0.512	0.676	5.97
	1596	16.83	0.506	0.696	5.93
	1597	17.64	0.518	0.695	6.35
	1598	16.86	0.508	0.695	5.95
	1599	17.19	0.511	0.686	6.02
	15910	16.99	0.508	0.697	6.02
	15911	16.48	0.510	0.693	5.82
	15912	17.11	0.514	0.713	6.28
	15913	17.09	0.509	0.676	5.89
	15914	16.23	0.489	0.670	5.32
	15915	15.55	0.503	0.693	5.42
	15916	15.77	0.481	0.632	4.80
	15917	15.21	0.475	0.639	4.61
	15918	16.45	0.501	0.653	5.39
	15919	16.01	0.504	0.722	5.82
	15920	17.64	0.516	0.699	6.37
	15921	16.45	0.510	0.715	6.00
	15922	16.29	0.510	0.727	6.03
	15923	16.89	0.508	0.720	6.18
	15924	15.99	0.505	0.699	5.65
	15925	16.90	0.510	0.671	5.78
	15926	15.89	0.490	0.605	4.71
	15927	16.35	0.511	0.709	5.92
	15928	16.21	0.491	0.615	5.16
	Average	16.56	0.506	0.684	5.75 (8.34)*
Run 16-160 Graphite crucible M.C., Displaced Die	1601	15.57	0.503	0.709	5.55
	1602	15.16	0.491	0.611	5.54
	1603	15.73	0.506	0.704	5.60
	1604	14.62	0.487	0.557	3.96
	1605	14.54	0.491	0.553	3.95
	1606	16.14	0.514	0.691	5.73
	1607	15.85	0.501	0.527	4.18
	1608	15.04	0.496	0.673	5.02
	1609	17.56	0.504	0.724	6.40
	16010	15.89	0.496	0.670	5.28
	16011	16.75	0.503	0.726	6.11
	16012	16.40	0.504	0.688	5.69
	16013	15.82	0.507	0.678	5.44
	16014	16.38	0.502	0.633	5.21
	Average	15.82	0.500	0.653	5.19 (7.53)*

* Numbers in parentheses are the projected values assuming 45% power gain on AR coating.

Legend: (a) Growth run number
(b) Crucible type: G = graphite, Q = quartz
(c) Die top: F = flat, D = displaced
(d) Capillary configuration: MC = multicapillary
SC = saw-cut

L_n (μm)

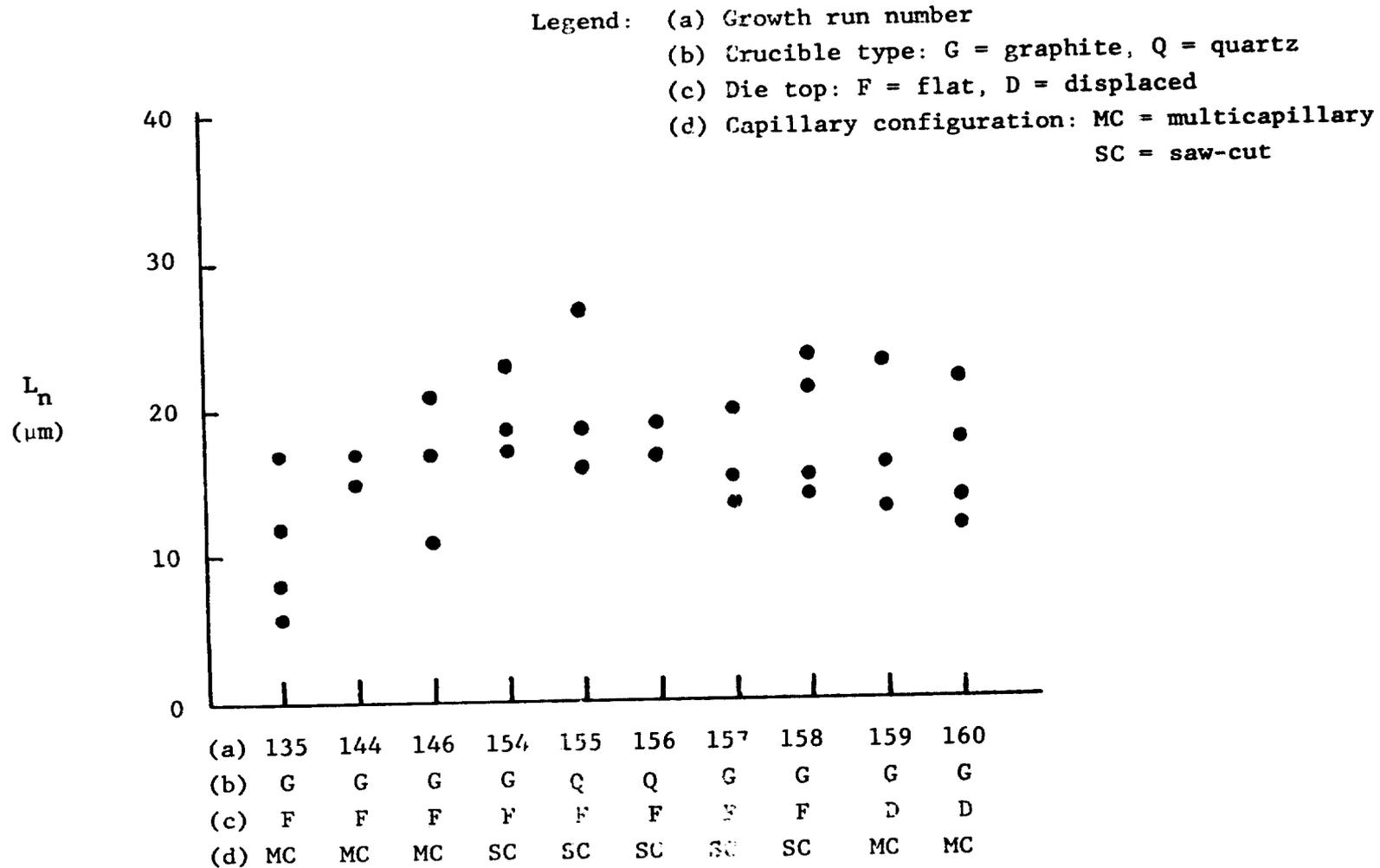| (a)	135	144	146	154	155	156	157	158	159	160
(b)	G	G	G	G	Q	Q	G	G	G	G
(c)	F	F	F	F	F	F	F	F	D	D
(d)	MC	MC	MC	SC	SC	SC	SC	SC	MC	MC

Fig. 10. Summary of diffusion length data for ribbon material from furnace No. 3A.

whose magnitude frequently is hard to evaluate unless significant numbers of comparative measurements using different methods are made. MTSEC is engaged in trying to clarify the situation both within and outside this particular program. In the meantime, however, the data and their cross correlations have to be treated with caution and the only truly reliable guide to progress is the absolute performance of solar cells in the desired size.

VI. REFERENCES

1. F. V. Wald et al., "Large Area Silicon Sheet by EFG,"
   Annual Progress Report, DOE/JPL 954355/78-3 (February 1979).

2. F. V. Wald et al., "Large Area Silicon Sheet by EFG,"
   Monthly Progress Report for period Oct. 1 - Oct. 31, 1978,
   DOE/JPL 954355 (November 1978) p. 10.

VII. APPENDICES

1. **Updated Program Plan**

   The program plan shown previously is still in effect.

2. **Man Hours and Costs**

   Previous cumulative man hours were 54,198 and cost plus fixed fee was $1,913,433 through the third quarter of 1978. Man hours for the fourth quarter of 1978 are 7,015 and cost plus fixed fee is $252,721. Therefore, total cumulative man hours and cost plus fixed fee through December, 1978 are 61,213 and $2,166,154, respectively.

3. **Engineering Drawings and Sketches Generated During the Reporting Period**

   None.

4. **Summary of Characterization Data Generated During the Reporting Period**

   See Section V, in particular Table V which demonstrates achievement of large area (7.5 x 7.5 cm^2) cells with efficiencies of ~9% at AM1.

5. **Action Items Required by JPL**

   None.

6. **New Technology**

   None.

7. Preprint, "High Speed EFG of Wide Silicon Ribbon," by J. P. Kalejs, B. H. Mackintosh and T. Surek. Submitted to Journal of Crystal Growth for publication.

APPENDIX 7

"High Speed EFG of Wide Silicon Ribbon," by J. P. Kalejs,
B. H. Mackintosh and T. Surek. Submitted to Journal of
Crystal Growth for publication.

HIGH SPEED EFG OF WIDE SILICON RIBBON

J. P. Kalejs, B. H. Mackintosh and T. Surek*

Mobil Tyco Solar Energy Corporation
16 Hickory Drive
Waltham, Massachusetts, 02154, USA

A system for high speed EFG of silicon ribbon is described which is capable of growing ribbon up to 7.5 cm in width and 7.5 cm/min in speed. A technique for achieving constant width growth has been developed through the utilization of temperature gradients along the ribbon width to stabilize and control the ribbon edge. Problems which have to be solved with respect to maintaining growth stability and eliminating buckling of the ribbon at higher growth speeds are examined in detail.

*   Present address: Photovoltaics Program Office, Solar Energy Research Institute, 1536 Cole Boulevard, Golden, Colorado, 80401, USA

1. INTRODUCTION

The development of the Edge-defined Film-fed Growth (EFG) system for silicon ribbon has been directed toward attainment of increased area throughput rates as part of an effort to meet manufacturing goals of 50 cents a peak watt for silicon ribbon solar cells by 1986[1]. The present level of EFG ribbon pilot production technology is capable of attaining rates of approximately 5 cm^2/min in single ribbon furnaces. The development effort aims to increase the rate by a factor of about twenty through the utilization of multiple ribbon furnaces, in which up to five ribbons are grown simultaneously. Two key elements of this program require that ribbons be grown at widths of up to 7.5 cm while simultaneously achieving speeds of 7.5 cm/min. The basic requirements for an EFG system to achieve these targets of width and growth speed and problems that must be solved as the speed and width are increased are the topics of this paper.

Considerable progress has been made in recent years in the understanding of the fundamentals of crystal growth by the EFG technique [2]. Practical application has had the most success in growth of sapphire [3] and silicon [4]. Interest in silicon EFG in the form of ribbon for manufacture of low cost solar cells for terrestrial applications has accelerated the development of ribbon growth technology. At the same time, studies of structure and electronic properties of ribbon grown at speeds of up to 2.5 cm/min and widths of 2.5 cm have shown that acceptable material quality is readily achieved for these growth conditions [4]. Consequent demand for higher ribbon area throughput rates to achieve significant cost reduction for solar cells requires growth of yet wider ribbon at even higher speeds. It remains to be demonstrated that acceptable material quality will be maintained with the increased complexity in the EFG system and more extreme growth conditions necessary at the higher throughput

2

rates to be realized.

The goals of speed and width each bring important constraints to bear on silicon ribbon EFG system design. On the one hand, the increase in growth speed demands the removal of the latent heat of crystallization from the growth interface at rates greater than would be practical through radiation alone. A means which has been adopted to enhance this heat loss is the use of water-cooled heat removal elements aided by helium gas conduction. However, forced cooling of the growth interface at the levels required leads to the generation of stress which the typically thin (100 to 200 μm) ribbon desired cannot withstand. To alleviate this condition, annealing afterheaters are provided; these reheat the ribbon to relieve stresses and permit more gradual cooling of the ribbon to room temperature.

In order to grow ribbon at increasing widths, while at the same time maintaining high growth speeds, an understanding is needed of the mechanisms of ribbon edge position control and stability. This is especially important for the development of a multiple ribbon growth capability. Considerable insight is provided in this area through the flexibility afforded by EFG die design. In many situations, active die-top temperature control, defined here as selective heating of the die top by means of auxiliary heaters or cooling by directed gas flows, provides indispensable supplementary aid in furthering the practice of controlled, stable growth.

A high speed EFG system for wide silicon ribbon is described in Section 2. Sections 3 and 4 examine, respectively, the state-of-the-art level of understanding of ribbon edge position control and stability and the causes of stress related problems and their control. In Section 5, we briefly examine effects of speed and width on material quality.

2.   EFG SYSTEM FOR WIDE, FAST GROWTH

An EFG system which is to provide an environment conducive to high speed growth of wide silicon ribbon must meet several requirements: (1) it has to provide for the removal of the latent heat of crystallization from the growth interface; (2) it should achieve stress relief in the ribbon; and (3) it should allow a means of adjustment of the die-top isotherms so that the ribbon edge position can be controlled and stabilized.   Such a system has been incorporated into the cartridge concept at Mobil Tyco.   All the essential control elements for these tasks as well as the EFG die are housed in a self-contained unit, or cartridge.   This cartridge can be decoupled and removed from the furnace main zone, containing the crucible and bulk melt, during furnace operation.

2.1   Cartridge Description

A discussion of the cartridge concept of crystal growth has appeared in a previous report [1] and will not be repeated here.   The system components contained in a cartridge used for high speed growth of 7.5 cm wide ribbon are illustrated in schematic cross section in fig. 1.   The cooling and heating elements for vertical and die top temperature control, as well as the die, are housed in a graphite enclosure consisting of four walls and a floor.   The walls are attached at the top of the cartridge to water-cooled stainless steel positioning blocks.   The walls and floor perform a very important function in providing for critical alignment of the die top relative to all the system components interior to the cartridge.   These include (from the cartridge floor up) the die heaters, die-top radiation shields, the water-cooled heat removal element, a second set of radiation shields, and linear cooling plates containing the afterheater.   The growth slot, through which the ribbon is pulled, is lo-

cated central to the linear cooling plates and is typically 0.15 cm wide. The separation between the die top and the maximum temperature point of the after-heater is approximately 2 cm.

The steep temperature gradient (up to 2500°C/cm in the solid near the growth interface) necessary for high speed growth (~ 7.5 cm/min) is established through the combined action of the die heaters, the die top radiation shields, and the heat removal elements. The latter also contain gas flow channels which direct gas onto the ribbon surface in very close proximity to the growth interface. When a high thermal conductivity gas, such as helium, is passed through the heat removal elements, their cooling capability is greatly enhanced.

Ribbon exiting from between the heat removal elements has generally undergone large amounts of plastic deformation because of the nonlinear decrease in temperature with distance above the growth interface throughout this region. If the ribbon were continued to be cooled to room temperature, it would generally contain large residual stresses which frequently lead to the ribbon fracturing. In order to minimize the residual stress in the ribbon, it is therefore reheated to temperatures (≳ 1200°C) above which complete stress relief can occur on the time scale of the growth, and then it is cooled in a linear temperature profile in passing between the linear cooling plates.

In a typical growth configuration, up to 4 or 5 cm of the die extends a-bove the level of the bulk melt into the cartridge. If the melt (main zone) heater were the only adjustable parameter to keep the die-top temperature near that of the melting point of silicon, severe overheating of the melt in the crucible would result. In order to avoid this situation, and also to provide a means of altering the die-top isotherm shape, additional heating is provided by die heaters, described in the following section.

5

2.2 Die Top Isotherm Control

The die-top thermal field is maintained by the action of a number of cart-
ridge components. Experimental results, discussed in Section 3, show that there
is a definite correlation between the die-top thermal field and the ability to grow
ribbon in a stable manner. By far the most important elements in establishing
and maintaining the appropriate die-top isotherms are the design of the die itself
and the die heaters. Their functions are described in more detail below.

The EFG die shapes the cross section of the growing crystal. Considerations
of the factors which produce stable meniscus configurations for silicon ribbon
growth with graphite dies have appeared elsewhere [2,4]. The present discussion
will deal with the manner in which specific aspects of the die design, namely,
the nature of the die-top contour and the capillary geometry, affect the die top
temperature field.

In the case of graphite dies, considerable flexibility is available in the
choice of the shape of the die-top contour. The results presented here will be
mainly for nominal 7.5 cm wide ribbon grown from dies of the type shown in Fig. 2.
The die-top flat width (which is uniform), the top slot dimensions, and the capil-
lary feed slot geometry are considered as design variables. The utility of
notches near the die ends is discussed below. Differences in growth conditions
can be expected if the die top is contoured, such as by cutting a radius in the
flat top die shown. In this situation, the die flats can be made either uniform
or nonuniform in width. Growth conditions encountered with this type of die will
not be discussed here, since they are not considered to add to the present dis-
cussion of stability. However, they do find practical application in other
ribbon growth situations and their use has been discussed elsewhere [4].

Cross sections taken through the die illustrate several capillary config-
urations in Fig. 3. The thermal conductivity of liquid silicon is approximately
twice that of the graphite typically used in silicon ribbon growth. In addition,
melt flow continuously brings hot melt to the die top and interface region. For
these reasons, the extent of melt penetration of the die top allowed by a par-
ticular die design has bearing on the die top isotherm shape.

The choice of die heaters is dependent on the crystal growth geometry and
the design of die which are to be used in a particular application. For ribbon
growth with a cartridge, it has been found advantageous to heat each end of the
die separately from its central part by means of individually controlled heaters
[1]. In this arrangement, the heater for the central section, or face heater,
supplies the bulk of the power. Its level of heating is maintained via closed
loop feedback from a thermocouple positioned near the die face. The end heaters
are used mainly in a "trimming" mode, that is, to supply enough power only to
control the ribbon edge isotherms. A configuration of end and face heaters used
to routinely grow 7.5 cm wide silicon ribbon is shown in Fig. 4. Here, the end
heaters are "U"-shaped and are designed to be most effective over a 1 to 2 cm
span at each die end.

3.   RIBBON EDGE POSITION CONTROL AND STABILITY

This section discusses ribbon edge position control and stability during
growth. Only limited understanding of the shape of the die top isotherms which
promote spreading of narrow ribbon and stable growth of wide ribbon at a pre-
selected width is available at this time. An examination of the die top and
ribbon thermal conditions deduced from a one-dimensional qualitative heat transfer
model is presented first. An attempt is then made to relate this model to experi-

mental data on the thickness profiles across the width for 7.5 cm wide ribbon grown under steady-state conditions. Finally, the role of die design as it relates to experimental observations of ribbon edge position control and stability will be examined.

3.1 Heat Transfer Considerations

The environment of the meniscus and growth interface is extremely complex from a heat transfer point of view, and a full three-dimensional analysis has not been attempted to date. However, some insight into the factors affecting ribbon edge stability may be gained from examination of a one-dimensional model of heat transfer in a growing ribbon. The present discussion is based on an approach which has previously been used to successfully correlate ribbon thickness to meniscus height and growth speed [5].

Idealized temperature profiles in a one-dimensional model of heat flow in the ribbon and in the liquid melt between the growth interface and die top are sketched in Fig. 5 for static seeding as well as for typical growth conditions. The effects arising from variation of medium properties with temperature, the changing cross section of the melt and radiation from the meniscus surface are neglected for the moment. Case 1 corresponds to the situation, during static seeding, where the ribbon or seed of a given thickness is contacting the melt and a meniscus of vertical height s is formed. The temperature gradients in the solid and liquid, G_S and G_L , respectively, satisfy the heat flux balance relation $k_S G_S = k_L G_L$; k_S and k_L are the respective thermal conductivities of solid and liquid silicon ($k_L \simeq 3 k_S$). During startup of growth, this balance is disrupted by a release of heat of crystallization $\rho L V$ at the solid-liquid interface; ρ is the solid density, L the latent heat of fusion per unit mass and V the growth velocity.

The additional heat removed by convection by the growing crystal lowers the temperature gradient in the solid only slightly for the dynamic growth situation, as shown by case 2 in Fig. 5. For heat balance, and in order to maintain the meniscus height at s and the original ribbon thickness, the die-top temperature must be lowered to T_G during growth from that for static seeding, T_S.

In practice, a one-dimensional picture of heat transfer during ribbon growth is inadequate because the meniscus height will vary across the ribbon width, and, in most situations, the ribbon thickness correspondingly is also not constant. Within the context of the above assumptions, this more complicated situation can be solved by performing similar heat flux balances at every point along the ribbon width. The temperature gradient in the solid will be a function of the ribbon thickness, t , of the form $G_S \sim t^{-\frac{1}{2}}$ [5]. Under stable growth conditions with the die shown in Fig. 2, the meniscus height at the ribbon edge is smaller than that found near the center, and the ribbon thickness is accordingly greater. In principle, the same heat flow balance can be performed at the ribbon edge. However, there is an additional competing effect influencing the temperature profiles very near the ribbon edge which must be taken into account: for a given ribbon thickness profile, the edge will have a greater surface per unit cross-sectional area than the ribbon center. This increases the radiative heat losses (both from the solid and from the meniscus surface) at the edge above those found at the ribbon face.

Two possible temperature profiles for the ribbon edge under dynamic conditions are shown as Cases 3 and 4 in Fig. 5. With the typically lower meniscus height, s_1 , and thicker ribbon, the one-dimensional heat transfer model predicts a lower temperature gradient in the solid near the ribbon edge, and hence a lower die-top temperature than near the ribbon center. This would lead to

9

steady-state growth as shown by Case 3. On the other hand, if competing radiation losses due to an increased surface area at the ribbon edge became dominant, the temperature distribution could be expected to be as shown in Case 4. The experimental results described below seem to indicate that steady-state growth in the present system takes place with temperature profiles at the ribbon center and edge as represented in Fig. 5 by Cases 2 and 3, respectively.

3.2 Die Top Temperature Profile

Routine growth of 7.5 cm wide silicon ribbon with the cartridge system described above has permitted the experimental study of conditions which promote ribbon edge stability. Measurements of ribbon thickness as a function of width have provided the experimental data in lieu of direct temperature measurements. The latter are particularly difficult to perform reliably with thermocouples without disruption of the die top thermal field for the die designs in use.

Typical thickness profiles across the width of the ribbon are shown in Fig. 6 for steady-state growth at constant width with the die and die heater configuration of Fig. 4. Each trace represents a ribbon grown from a separate seeding but all are grown from the same die and melt. The main features of the ribbon thickness profiles, such as the rapid increase in thickness at the extreme ribbon edges and the minima at locations about 1 cm from each ribbon edge, were reproduced with several different die and end heater configurations. The die-top contour shape and end heater cross section (hence, distribution of radiative heating) were deliberately varied in order to explore the range of stable growth conditions available [6]. It was concluded from observations that ribbon edge stability during growth of wide ribbon in this system is optimum for a general shape of thickness profile illustrated in Fig. 6.

Except very near the ribbon edge (within about 0.1 cm), the thickness profile is expected to mirror the temperature distribution across the die top; that is, one-dimensional heat transfer relations should be applicable. Independent observations of the meniscus height variation under static seeding conditions as well as studies of die top freezing patterns both suggest such an inference to be valid. The die top isotherm shapes for the die and heater configuration shown in Fig. 4 deduced from these observations are sketched in Fig. 7. With zero end heater power, the face heater heats the die center more than the ends. Growth of full-width ($\gtrsim$ 7 cm wide) ribbon with the resulting isotherm shape, shown in Fig. 7(a), is difficult because the temperature difference from die center to edge necessary to maintain the ribbon edges stable near the ends of the die is generally too large to support satisfactory, stable growth. In this case, either the center of the ribbon thins to where a meniscus no longer can be maintained, or the die ends become so cold that the ribbon edges are prone to frequent freezes.

At the level of end heater power typical of full-width steady-state growth, the isotherm shape of Fig. 7(b) results. Overlap of the areas of heating of the face and end heaters creates a local hot region about 1 cm from each die end. This also increases the lateral temperature gradient as the die edge is approached. The notches in the die top (see also Fig. 2) tend to modify the steepness of the temperature decline at the extreme die ends. The die top isotherm shape under dynamic conditions just described corresponds to the temperature profiles of Cases 2 and 3 of Fig. 5 at the ribbon center and edge, respectively.

3.3 Thermal Mechanism for Edge Control and Stability

It is concluded from the profiles of Figs. 6 and 7 that the ribbon edge location for most stable growth is associated with a region of a steep lateral

11

temperature gradient and decreasing temperature relative to the rest of the die top. The natural tendency of the ribbon edge, when placed in such a temperature gradient, would be to move, or "spread", toward the region of the lowest temperature. However, in the present situation, this spreading tendency is counteracted by radiative heating of the die end and ribbon edge by the end heater, which acts to reduce the lateral temperature gradient near the die end. The ribbon edge can thus be locked into a very stable position by end heater adjustment alone, provided the edge position remains in a region of decreasing temperature.

The degree of effectiveness of this thermal edge stability mechanism appears to be enhanced by the presence of both the region of overlap of heating of the end and face heaters and the die end notches, which together tend to form a thermal "well". Confinement of the ribbon edge in this well promotes more stable growth than is possible simply by positioning in a region of uniformly decreasing lateral temperature. The most stable growth occurred with the ribbon edge very close to or encountering the inside edge of the notch. For the notch widths of less than about 0.03 cm used, its presence did not appear to markedly affect the spreading rate of the ribbon as it encountered the notch edge. The ribbon edge also did not show preference for growth in any given location in the neighborhood of the notch. The influence of the notch on ribbon edge stability thus appeared to be mainly thermal for this die design.

Thickness profiles described in the previous section have also been used to obtain information on the response of the steady-state meniscus configuration to changes in growth speed and hence on effects of changes in speed on growth stability. Figure 8 shows typical data for a single ribbon growing continuously but subjected to increases in pulling speed. After constant width growth at a

width of 7.4 cm and a speed of 3.4 cm/min had been established (trace 1), the pulling speed was suddenly increased to 3.8 cm/min. This raised the meniscus height and the ribbon edge started to taper and the ribbon to grow thinner. Initially, no adjustments other than the speed increase were made, and the taper decreased the ribbon width from 7.4 to 7.2 cm. Steady-state, constant width growth reestablished itself after about 5 cm of growth without the necessity of heater power level adjustments. Growth at a constant width of 7.4 cm was then restored at this speed (trace 2) by adjustment of the power level of each end heater. A further increase in speed from 3.8 to 4.7 cm/min resulted in a decrease in the ribbon width from 7.4 to 6.8 cm over about 8 cm of growth. Constant width growth at 7.1 cm was reestablished by adjustment of the end heaters (trace 3).

The ribbon edge position control and stability exhibited above demonstrate important aspects of width control which are required for successful operation of multiple ribbon furnaces. In regard to the first of these, the ability to control the ribbon edge position by end heater adjustments alone makes it attractive to incorporate the latter into an automated system for maintaining constant width growth. This system could then be expected to cope with fluctuations in growth speed or meniscus height, such as result from ribbon environment and die top temperature variations. On the other hand, stability of the ribbon edge against deliberate growth speed increases affords the possibility of achieving much higher growth rates in a continuous manner. Stable and reproducible constant width growth has been demonstrated in the speed range from 3 cm/min to 5 cm/min. Speeds up to 7.5 cm/min have been attained with this same system, although only for short periods of time, while suggesting that the high speed capability of the cartridge even then may not be fully realized. However, routine growth above about 4 cm/

13

min is hampered by a problem of a different nature, ribbon buckling, which is discussed in Section 4 below. Buckling tends to lead to displacement of the ribbon at the growth interface and so destabilizes growth.

The ribbon thickness data at different growth speeds have been used to estimate the die-top temperature along the ribbon face and at the edge with the help of the one-dimensional heat transfer relations developed in Reference [5]. The results can be manipulated to express the difference in temperature between the die top (T_D) and the growth interface (T_M) as:

$$T_D - T_M = (s'/k_L) \left[\frac{af(\beta)}{t^{\frac{1}{2}}} - \rho VL \right] \tag{1}$$

where

$$s' = \frac{t \ln (t_D/t)}{(t_D - t)} \cdot s \tag{2}$$

Here, the interface gradient in the liquid meniscus is written $G_L = (T_D - T_M)/s'$, with s' related to the vertical meniscus height s by a geometric factor, as given in Eq. (2). This factor takes into account variations in temperature gradient in the meniscus due to changes in its cross section arising from differences in thickness between the ribbon, t , and the die top, t_D . The derivation of the geometric factor in Eq. (2) is discussed elsewhere [7,8]. The factor $a = (\sigma \epsilon k_M T_M^5)^{\frac{1}{2}}$, where k_M is the solid silicon thermal conductivity at the melting temperature T_M , σ is the Stefan-Boltzmann constant and ε the solid silicon emissivity. The function $f(\beta) = [1 - \beta^{-4} (1 + 4 \ln \beta)]^{\frac{1}{2}}$, with $\beta = T_M/T_o$, contains the adjustable parameter T_o , a temperature which characterizes the environment of the ribbon to which it loses heat through radiation. As a result of the simplification inherent in a one-dimensional model, T_o cannot be expressed in terms of known temperatures of the complex thermal environment surrounding the ribbon in cartridge growth. However, it can be estimated from the maximum growth speed capability of a given cartridge environment [5]. For the cartridge growth conditions used to obtain the

14

data in fig. 8, T_o is taken to be 1100^oK, which gives $f(\beta) = 0.7$.

Average ribbon thicknesses, both for a 5 cm span in the central part of the ribbon and at the ribbon edge, have been obtained from the data of fig. 8 and used as a basis for calculating $T_D - T_M$ for three growth speeds with the help of Eqs. (1) and (2). The results are given in table 1. The tabulated meniscus height values typical of the ribbon face are taken from calculated meniscus profiles [2,5]. Equivalent results for the ribbon edge meniscus height are not available. The numbers given in the table represent estimated average values of the meniscus height within a 0.5 cm span at the ribbon edge. For reasons already discussed in Section 3.1, the one-dimensional heat flow balance assumed in the derivation of Eq. (1) may no longer be valid at the ribbon edge. Thus, the relevant $T_D - T_M$ values given in table 1 should be taken as indicating the trend of die-top temperature in a qualitative sense only.

Experimental observations combined with the calculated die-top temperature values given in table 1 can be used to further the understanding of factors which promote stable growth as speed is increased and in judging the growth speed capabilities of a given system. For example, increasing dominance of the latent heat contribution to heat flow in the meniscus leads to the decrease in die-top temperature seen with a speed increase from 3.8 cm/min to 4.7 cm/min, as compared to the inverse dependence below 3.8 cm/min (see table 1). In the case of $T_D = T_M$, the latent heat contribution becomes sufficiently large so as to reduce the temperature gradient in the meniscus to near zero. The growth interface is then no longer constrained from moving toward the die top, and freezing of the ribbon to the die top is likely to occur. Such frequent freezes were experienced in attempts to raise the speed above 4.7 cm/min during the experiments from which the data of

fig. 8 were obtained; these observations were the basis of assigning the charac-teristic environment temperature $T_o = 1100^{o}K$ for the system. Solution of Eq. (1) for the ribbon thickness which can support a maximum growth speed of 4.7 cm/min with $T_o = 1100^{o}K$ ($\beta = 0.7$) gives $t = 0.043$ cm. This is very close to the measured maximum ribbon thickness of 0.040 cm occurring near the ribbon edge, and suggests that heat losses along the thickest part of the ribbon are the limiting factor in preventing achievement of higher growth speeds for the given ribbon thickness pro-file and cartridge cooling environment. The good agreement between the calculated limiting thickness and the measured maximum ribbon thickness also gives support to the use of the one-dimensional model heat transfer equation in close proximity to the ribbon edge, hence to the method of deducing die-top isotherm shape from thick-ness profiles across the ribbon width.

The unavoidable uncertainty in the die-top temperature differences cal-culated at the ribbon edge at present arises from the difficulty in assigning appropriate value to the meniscus height there. The average values used in table 1 lead to an upper limit for the temperature differences $T_D - T_M$ at the ribbon edge since the meniscus height appears to always have its minimum height at the extreme edge. These minimum values are generally from thirty to sixty percent of the meniscus heights for the ribbon edge given in table 1. The calculated $T_D - T_M$ values given for the ribbon edge therefore underestimate the temperature decreases as the ribbon edge is approached. As observed earlier in the discussion of ribbon thickness profiles, most of this decrease takes place within about 0.5 cm of the ribbon edge.

Explanations of the observed responses of the ribbon edge location to increases in growth speed and end heater adjustment discussed above appear to be beyond the scope of the one-dimensional heat transfer model utilized here. The

experimental observations suggest that the lateral temperature gradient in the neighborhood of the ribbon edge, which is expected to be affected by these changes, is an important factor in promoting ribbon edge stability. Understanding of the nature of these responses will require a model which can account for the effects of variations in meniscus height and temperature in the ribbon width dimension on die-top isotherm shape.

3.3 Die Design Influence On Isotherm Shape

Measurements of ribbon thickness profiles have provided valuable information regarding thermal conditions promoting ribbon edge stability during wide silicon ribbon growth. The die design used in this investigation (fig. 2) was used for the simplicity afforded by a planar die top. Nevertheless, the available choices in die, as well as heater, designs offer a wide range of options for shaping die top isotherms, hence the ribbon thickness profile; other configurations have been used with varying degrees of success in the growth of silicon ribbon [2,4,6]. By way of example, the following discussion will focus on specific illustrations of how die design changes which alter the melt flow configuration affect ribbon thickness profiles, and ultimately growth stability.

The three capillary feed geometries shown in fig. 3 have been used in the study of growth stability of wide ribbon. The most straightforward geometry from a heat transfer point of view would supply the melt uniformly to the interface, such as by a capillary slot extending across the full width of the growing ribbon. This becomes less practical to do with increasing width. Splaying or warping of the die then becomes a problem, since it becomes difficult to maintain a uniform die top slot width when the die tips on either side are not connected at intervals.

The open channel die of fig. 3a provides a practical compromise. While melt flow to the meniscus is partially restricted, heating of the die top by liquid silicon is predictable, although not uniform. At the same time, die fabrication is simplified. The capillary slots are formed from saw cuts. The die top is usually a single piece of graphite. This reduces the possibility of warping. Melt supply to the meniscus by means of various arrangements of circular capillaries, examples of which are shown in figs. 3b and 3c, is again made attractive through the simplicity of the fabrication. With this latter melt flow geometry, regions of the meniscus located directly above capillary exits are preferentially heated by silicon melt drawn up through the die. Growth stability was not noticeably affected by the resulting isotherm shifting at the lower growth speeds of interest here, viz., 2 cm/min to 3 cm/min. However, at higher speeds this is no longer the case, and significant changes in die top isotherm shape, as reflected in ribbon thickness variations, arise as a result of heating by melt in capillary exit regions. The open channel die of fig. 3a now offers several clear advantages over the other designs. First, the wider melt flow channel allows mixing of melt over more of the die width, thus smoothing out temperature variations arising from the melt flow. Further, the die top isotherms are modified so as to enhance thermal ribbon edge stability as a result of an increase in the temperature gradient from the die center to the edges because of the melt heating primarily the die center. On the other hand, die top isotherm inhomogeneity induced by melt heating for the die geometries of figs. 3b and 3c can be expected to become more severe as speed increases, and will tend to exert a destabilizing influence on growth stability. An additional disadvantage of these geometries is associated with silicon carbide growth on the interior walls of the capillaries. Individual capillaries of the type shown appear to be more prone to blockage by

silicon carbide particles than wider dimension capillary slots. Silicon carbide growth of the exits of the vertical capillaries to the top slot for a die of the design illustrated in fig. 3c is shown in fig. 9. The asymmetric melt flow and unbalanced die top heating arising in such situations are suspected to contribute to instability of wide ribbon growth from these dies.

4. Thermal Stress Related Problems

This section discusses some thermal stress-related problems which have been observed in wide and fast ribbon growth. As illustrated by the photographs in figs. 10 and 11, these problems are: (i) occasionally high residual stresses in the ribbon which show up in problems of cutting it into solar cell blanks; and (ii) large deviations (buckles and ripples) of the ribbon from flatness which make the ribbon useless for cell fabrication. In this section, the possible causes of these problems are reviewed, and ways in which they are addressed in the EFG system described above are examined. The emphasis here is to present the under-lying physical phenomena responsible for the observations, and to identify in a qualitative manner the effects of appropriate experimental variables whose control can lead to their resolution.

In the following subsections, we examine the origin of thermal stresses in EFG silicon ribbon, discuss the relaxation of these stresses by plastic flow and the problem of residual stress in the ribbon, consider the fundamental physical phenomena in buckling of ribbon, and review the status of the ribbon growth experiments insofar as these stress-related problems are concerned.

4.1 Origin of Thermal Stresses in Ribbon EFG

A principal distinguishing feature of ribbon EFG is the rapid growth rate attainable as a result of the large surface-to-volume ratio of the ribbon, which

19

enhances the removal of the latent heat of crystallization from the growth interface. The deleterious effect of such rapid heat loss from the ribbon surface, however, is the generation of nonuniform temperature gradients in the ribbon; these give rise to large thermal stresses during growth.

The origin of these thermal stresses is readily understood from a simple analysis of the process of cooling the ribbon from its point of freezing to room temperature. During cooling, each ribbon element contracts proportionally to its own temperature fall. If adjacent elements contract differently, they will restrain each other's contraction and thermal stresses result. By considering the ribbon as consisting of adjacent longitudinal elements, it can be readily seen that the contraction of such adjacent elements will be unrestrained if the ribbon is in a uniform temperature gradient, provided that the thermal expansion coefficient is independent of temperature; under these conditions the ribbon will be stress free. If the ribbon is in a nonuniform temperature gradient, however, lateral deformation in the plane of the ribbon must occur in order for adjacent elements to fit together. Thus, thermal stresses, which will be proportional to the amount of bending that must be imposed to fit the elements together, are generated in the ribbon. These stresses will increase with increasing curvature of the temperature profile (i.e., proportionally to d^2T/dx^2, where the x-coordinate is along the direction of ribbon pulling) and with increasing ribbon width. The important point to note from this qualitative argument is that, in any crystal growth situation, it is impossible to cool the ribbon to room temperature without developing thermal stress in the ribbon at some point.

Thermoelasticity theory [9] can be used to predict the dependence of the thermal stresses on the ribbon width and on the temperature profile along the length of

the ribbon (i.e., the vertical profile) and on that across the ribbon width (i.e., the horizontal profile). The complete theoretical analysis for thermal stresses in ribbons is given elsewhere [10]; some recent numerical calculations are presented in this volume [11]. For the present, we are only interested in the normal stress component σ_{xx} which acts along the length of the ribbon; below, we examine the qualitative dependence of this stress on the nature of the vertical and horizontal distributions in the ribbon and on position across the width of the ribbon.

Figures 12a and b show, respectively, the variations of σ_{xx} with distance from the growth interface and with the position coordinate y across a ribbon of width w, for a temperature distribution in the ribbon which is a function of the vertical coordinate x only. The specific temperature distribution and the other conditions assumed in the calculation are indicated in the figure caption. At the growth interface (i.e., x = 0), we must have σ_{xx} = 0. Furthermore, the nature of the σ_{xx} - distribution across the width of the ribbon at any position x is such that it is "self-equilibrating" (i.e., no net forces or moments). The distribution where the center of the ribbon is under tension and the edges are under compression (denoted by C-T-C in the following) obtains when the vertical temperature distribution is such that $d^2T/dx^2 > 0$ (e.g., see fig. 12b); the opposite situation (i.e., a T-C-T distribution) results when $d^2T/dx^2 < 0$.

The effects of nonuniform horizontal profiles on the thermoelastic stresses in the ribbon have also been considered theoretically [10]. It was found that σ_{xx} is compressive near the edges (i.e., a C-T-C distribution) for "smiling" isotherms, i.e., where the edges of the ribbon are hotter than the center at the same distance from the die. "Frowning" isotherms in the ribbon, on the other hand, result in a T-C-T longitudinal stress distribution, which would tend to counteract

the thermal stresses caused by the usual vertical cooling profiles where $d^2T/dx^2 > 0$.

There are two significant sources of horizontal temperature variations in silicon ribbon EFG as illustrated by the discussion of thermal fields in the previous sections. One arises from the fact that the ribbon width is finite; hence there are heat loss or gain variations across the ribbon width as a result of both ribbon edge effects (e.g., surface area/volume considerations) and asymmetries in the thermal environment across the ribbon width associated with the location and design of cooling or heating elements in the cartridge. The second, and equally important, source of nonuniform horizontal profiles arises from the grown-in thickness variations across the width of the ribbon (see Section 3.2). These thickness variations were shown to reflect temperature variations across the width of the die. For the same cooling environment, a thick ribbon tends to cool more slowly than a thin ribbon, and this contributes to increasing horizontal temperature variations across the width of the ribbon.

The effect of increasing the ribbon width is to increase the thermal stress in the ribbon; the stress component σ_{xx}, for example, increases approximately as the square of the ribbon width [10].

The treatment of thermoelastic stresses in the ribbon in the manner discussed above has only limited applicability. The analysis predicts the stresses which would exist in the ribbon at any point during growth if relief of these stresses were not permitted to occur. Thus, the ribbon either breaks in a region where the thermal stresses are too high, or it emerges at room temperature with no residual stress. In any practical growth situation, however, some form of stress relief occurs, as exemplified by the residual stress and buckling manifestations

illustrated in figs. 10 and 11. The mechanisms of stress relief which are of primary concern are the relaxation of the thermal stresses by plastic deformation processes and the stress relief by buckling. These are the subjects of the next two subsections.

4.2 Stress Relaxation by Plastic Deformation; Residual Stress in the Ribbon

At temperatures above about $600^{\circ}C$, plastic deformation processes such as the glide and climb of dislocations have been observed to occur in silicon crystals [12]. Plastic deformation by these mechanisms acts to relieve the thermal stresses described above during growth; the degree of stress relief at a given point in the ribbon may be complete or partial, depending on the time and temperature. Deformation by dislocation glide or slip is essentially instantaneous on the time scale of EFG ribbon growth; dislocation climb, on the other hand, requires the diffusion of vacancies, and hence the rate of stress relief by this mechanism is strongly temperature dependent.

It follows from the above that residual elastic strain (and stress) in the ribbon can be avoided if there is either complete relief of stress or no relief of stress (i.e., no plastic strain) during the entire time the ribbon is cooling from the melting point to room temperature. We are therefore concerned with the minimum time required, at various temperatures, to allow complete stress relief, or the maximum time during which no stress relief occurs. From experimental studies of stress relaxation in EFG ribbons, it has been concluded that, on the time scale of ribbon EFG, stress relief in the ribbon would be effectively complete at temperatures above about $1200^{\circ}C$, and that almost no stress relief would occur below about $600^{\circ}C$.

23

The above considerations suggest that the vertical temperature profile in the ribbon, ideally, should consist of three zones to permit fast growth of stress-free ribbon. The first zone (from the melting temperature to ~1200°C) should consist of an initially large temperature gradient (~2500°C/cm for a 7.5 cm/min growth rate), and a very rapid decrease of the gradient away from the growth interface; this is required in order to achieve the desired fast growth rate. Plastic strain in this zone should occur fast enough for the stress to be completely relieved. Of concern in this temperature region is the minimization of the plastic strain induced imperfections (e.g., dislocations). This can be achieved by minimizing the second and higher order derivatives of the vertical profile, or by countering the effects of the vertical profile with an appropriate horizontal profile, as discussed in the previous section. The second zone should be a region of constant temperature gradient in which the stress-free ribbon cools from ~1200°C to below ~600°C; no stress or strain is introduced in the ribbon in this zone. The third zone should consist of a further decrease in gradient that is needed to reach zero gradient at room temperature. No plastic deformation can occur in this latter zone; therefore, if the ribbon is stress-free when it enters it, it will again be stress-free when it leaves at room temperature. The crucial question in this third zone relates to the thermoelastic stress which is developed; if this stress does not fracture the ribbon, it will then disappear as the gradient becomes zero at room temperature.

The ideal vertical temperature profile described above is illustrated by curve (a) in fig. 13. The combination of the water-cooled heat removal elements and the actively heated linear cooling plates, described in Section 2.1, were designed to approximate this profile. The actual profile which is obtained in the experimental systems is shown by curve (b) in fig. 13. Basically, design and

fabrication limitations of the cooling zone arrangement chosen for the high speed cartridge virtually preclude the duplication of the ideal profile; invariably, the ribbon is "undercooled" to well below 1200°C before being reheated in the linear afterheater. The undercooling is undesirable in that it is likely to lead to a large number of dislocations, and it is also a likely contributor to the buckling problems described in the next section.

Finally, it should be noted that an analytic solution to either the problem of residual stress or that of defect density is exceedingly complex. The basic limitations to a useful solution lie in the insufficiency of plastic deformation data for silicon, and the complexity and nonuniformity of the crystalline structure of the ribbons.

4.3 Buckling of EFG Ribbons

In this section, we present a review of the fundamental physical aspects of buckling phenomena and the applications of these concepts to ribbon EFG. The discussion is qualitative in nature, and it attempts to identify the roles played by the various growth variables in EFG in buckle formation.

Buckling of the ribbon occurs in order to relieve the compressive stresses (i.e., $\sigma_{xx} < 0$) acting over a segment (or length) of the ribbon during cooling. Although buckling occurs as a result of an "elastic instability" under these compressive stresses, it can also occur in the temperature region ($\geq 600°C$) where plastic relaxation of stress can take place in silicon; when buckling occurs at high temperatures, it is not (or need not be) accompanied by the generation and motion of dislocations (i.e., by plastic flow). Whether buckling or plastic deformation acts to relieve the stresses at the higher temperatures depends on a number of factors, such as the magnitude of the stresses and the rate of stress

relief by plastic deformation (i.e., the time the ribbon spends at a given temperature during cooling). Whereas plastic relaxation is a gradual relief of thermal stress, stress relief by buckling is essentially instantaneous. In other words, buckling does not happen gradually, rather, the stresses must build up until a critical stress sufficient to cause buckling is reached over some ribbon length. The critical buckling stress is a complex function of the ribbon geometry (segment length, ribbon width and thickness) and of the nature of the normal stress distribution. The problem appropriate to the self-equilibrating σ_{xx}-distributions discussed in Section 4.1 has not yet been treated, as far as these authors are aware. By analogy to similar considerations in the literature [13], we expect that the functional relationship is qualitatively of the form:

$$\sigma_{cr} = A \frac{Et^2}{\ell^2 + w^2} \tag{3}$$

where σ_{cr} is the critical buckling stress, E is the modulus of elasticity, t is the ribbon thickness, w is the ribbon width, ℓ is a segment length of the ribbon, and A is a proportionality constant. This relationship predicts that the tendency to buckle is enhanced (i.e., σ_{cr} is lower) for wider ribbons, when long, thin ribbon segments are under compressive stress, and also at higher temperatures.

The quantity ℓ in the analysis is rather significant. A central feature of most buckling theories is that there exists a minimum length below which buckling cannot occur; at this length, the value of σ_{cr} is equal to the proportional limit or some other critical stress limit of the material. From our experimental observations of buckling, it appears that the relevant segment length ℓ is of the order of a centimeter or greater. Thus, it is of interest to consider only macroscopic features (i.e., those of dimension $= \ell$) of the ribbon cooling profile, rather than be concerned with the details of the temperature variation over shorter

distances. This aspect of buckling should aid greatly in making the problem experimentally tractable.

Buckling can relieve the stresses in the ribbon for either the T-C-T or C-T-C stress distribution described in Section 4.1. A T-C-T distribution is relieved by "center" buckling, as illustrated in fig. 14a; such buckling tends to elongate central elements and shorten edge elements of the ribbon. "Edge" or "torsional" buckling relieves a C-T-C stress distribution; in this case, one edge of the ribbon deflects upward, while the other deflects downward (see fig. 14b). In either case, one would expect the buckles to be periodic a-long the length of the ribbon; the periodicity will be determined by the length ℓ which is a complex function of the magnitude of the stresses and their variation along the ribbon length.

When buckling relieves the longitudinal stresses, it results in bending stresses in the ribbon, with the upper surface of a buckle being in tension and the bottom surface in compression. If buckling occurs at a high enough tempera-ture, these bending stresses may be relieved by plastic flow; otherwise, there will be residual bending stresses at room temperature. The presence (or absence) of residual bending stresses in a buckled ribbon can provide information as to the temperature region where buckling occurred.

If buckling were the only form of stress relief, i.e., if there were no stress relaxations by plastic deformation, the stresses of concern would be the thermo-elastic stresses discussed in Section 4.2. For this case, it can be readily argued that there can be no buckles remaining in the ribbon upon cooling; otherwise the ribbon will contain large residual stresses which would tend to flatten it.

If plastic relaxation of stress occurs, on the other hand, the unrelieved stresses at any point in the ribbon are a function of all the previous stress relief which has occurred as well as of the horizontal and vertical temperature profiles at the point in question. The growth rate enters the problem through its direct influence on the cooling profile within the ribbon, and, more importantly, through the way it affects the stress relaxation in a given temperature region (i.e., the time the ribbon spends at each temperature). If buckling has occurred, the stress caused by the buckle also has to be included in the determination of the existing stress distribution.

This discussion has been intended to demonstrate the extreme complexity of the problem. As indicated earlier, a useful analytic solution to this complex problem cannot be generated without considerable advancement in the understanding of plastic deformation phenomena in silicon; therefore, the approach to resolving the buckling problem in EFG ribbons has been primarily empirical. The status of the experimental efforts is summarized in the next section. For various ribbon cooling profiles, a qualitative determination can be made of the nature of the longitudinal stress distribution during cooling. From such considerations, it can be argued that the region of the vertical profile most critical to buckle formation is that between ~1200°C and ~600°C, where only partial relaxation of stresses by plastic flow occurs. Transitions between positive and negative curvatures in the vertical profile should be avoided in this region in order to minimize the probability for buckle formation. Horizontal temperature profiles are also an important factor in some of the current problems. There, it can be qualitatively argued that transitions from "smiling" to "frowning" isotherms are to be avoided. Of course, it should be possible to tailor the horizontal iso-

therms (especially in the afterheater region of the cartridge) in such a way as
to counteract the effects of nonuniform vertical profiles.

4.4 Experimental Observations of Buckling

In this section, a review of the status of buckle geometry characteriza-
tion and residual stress control is given. The interpretation of buckle patterns,
insofar as period, amplitude and type, is complicated by two factors. First, it
is difficult to resolve guidance-induced deviations from ribbon flatness (which
will be referred to as "ripples") from stress-induced ribbon buckling in the present
growth systems. Ripples are formed when deviations from ribbon flatness are either
initiated or propogated as a result of misalignment of the ribbon and the growth
slot or by faulty guidance in the pulling apparatus. Ripples appear in the repre-
sentative photographs in fig. 11 as straight-line demarcations across the full
width of the ribbon and are often non-periodic. The second complication in
buckle characterization results from superposition of buckles of different periods
and amplitudes, and the fact that interference from ripples often destroys buckle
periodicity.

The general features of two distinct types of buckle patterns typical of
7.5 cm wide ribbon grown in the speed range from 2.5 cm/min to 5 cm/min are illus-
trated by photographs and corresponding surface contour traces in figs 11a and 11b.
Each photograph is of a full-width ribbon of 40 to 50 cm length grown under steady-
state conditions at constant width. It is accompanied by three profilometer traces
taken on the same ribbon along the growth direction. The traces reproduce the
ribbon surface deviations from flatness along each ribbon edge and the ribbon
center. The patterns reproduced in fig. 11a are those typical of edge buckling,
where buckle formation alternates from one ribbon edge to the other along the

29

growth direction. The out-of-phase relationship of the alternating buckles is clearly evident from a comparison of the two traces taken along opposite ribbon edges. The center trace exhibits a more complicated surface contour variation, presumably arising from a superposition of the edge buckle patterns. The period of the edge buckles is approximately 8 cm. The patterns of fig. 11b illustrate center buckling; some interference, possibly from guidance or from edge buckling, shows up as a modulation of the background. The chief characteristic of the center traces is now an in-phase relationship between the buckles at each edge. The period of the center buckles varies from 2 to 3 cm.

Many features of buckle occurrence are qualitatively consistent with expected effects of the influence of growth parameters on the processes for buckle formation discussed above. Thus, buckling is most frequently observed in wide and thin ribbon (low σ_{cr}), in ribbon with nonuniform thickness (implying the existence of horizontal temperature gradients), and ribbons grown at faster rates (reflecting the influence of the vertical temperature profile). Nearly all ribbon grown with the cartridge described here at speeds in excess of 4 cm/min has been buckled, regardless of width. At speeds below 4 cm/min, the frequency of occurrence and characteristics of buckling are more unpredictable. Very often the buckles lack clear periodicity, or a definite center or edge character. Aside from interference between the buckles and the ribbon guidance system, the temperature and stress fields in the ribbon are extremely complex, and a given ribbon segment subjected to buckling stresses may vary in shape and extent. At the present time, sufficient data on temperature fields within the cartridge are not available to help identify which of the physical mechanisms of buckle formation discussed are operative in a given growth situation.

Finally, turning briefly to the problem of residual stress control, it has been shown experimentally that this stress can be satisfactorily controlled with the present afterheater and linear cooling plate design. For ribbon growth under steady-state conditions in the speed range from 2.5 cm/min to 5 cm/min, the maximum afterheater temperature can be maintained within a rather broad temperature range without increasing the residual stress at room temperature to measurable levels. The corresponding range of maximum temperatures attained in the ribbon is estimated to extend from about $1100^{\circ}C$ to $1300^{\circ}C$.

5.   Material Quality Considerations

Central to the development of an EFG system for growth of silicon ribbon with increased capacities for speed and width has been a concern that ribbon quality not be compromised. Ribbon grown at Mobil Tyco at speeds up to 2.4 cm/min and widths of 2.5 cm has been characterized with respect to structure and electronic qualities [4]. Ribbon grown from high speed systems of the type under discussion here exhibits distinct differences by comparison, in the appearance of a subsurface grain structure in the thickness cross section of the ribbon and an increase in material inhomogeneity [14]. The main difference between the two growth systems is the introduction of forced cooling and post-growth heating in the latter (see fig. 1). At present, there is no conclusive evidence to point to any specific effect as causing the differences in material properties of the ribbon grown in these two systems. However, it is conjectured that changes in interface shape accompanying increases in growth speed as well as differences in the ribbon thermal environment (both at the interface and above it) could be responsible for variations in material quality of the type observed.

6.   Concluding Remarks

The achievement of stable, constant width, growth and reproducible growth

conditions has demonstrated that EFG is a viable technique for high speed growth

of wide silicon ribbon. In the process, emphasis has been placed on gaining

understanding of die top isotherm configurations for which stable growth condi-

tions are realized. Success in this task allows questions relating to basic growth

phenomena, which are raised in Sections 4 and 5, to be answered through experi-

mentation. Several approaches which may prove to be of value in adding to the

understanding of factors which control ribbon quality and stress and buckle gen-

eration will now be examined briefly.

Interface shape has been demonstrated to play an important role in de-

termining material structure and impurity distribution within a growing crystal

in melt growth. At present, knowledge of the interface configuration during EFG

of silicon ribbon is lacking. However, the EFG die provides a unique opportunity

to address this problem. Due to its close proximity to the growth interface, the

shape of the latter is greatly influenced by the temperature distribution imposed

on the die. As has been noted, die top isotherms across the die width, particu-

larly, can be manipulated through changes in die top contour and capillary feed

geometries, or by active heater element utilization. On the other hand, cart-

ridge components which will affect the interface position and shape in the thick-

ness dimension are the die top shields, and the heat removal elements and after-

heater, which determine the cooling profile of the ribbon. However, it should be

recognized that thermal coupling among system components will often complicate

interpretation of the influence of a given component on interface shape.

For a given shape of growth interface, impurity transport by convection

or diffusion ahead of the interface may lead to redistribution of impurities across

both the thickness and the width of a growing ribbon. Theoretical considerations show that, in the range of growth variables considered here, the extreme aspect ratio of the ribbon (width much greater than thickness) favors melt impurity transport to be diffusion controlled across the ribbon thickness, but convection controlled in the width dimension [15]. Since die geometry can be used to influence the melt flow patterns ahead of the growth interface, this could also allow manipulation of the levels of certain impurities across the ribbon width dimension. Variations in capillary feed geometry have been noted in Section 3.3 to influence die top isotherm shape; therefore, they can be expected also to affect the shape of the growth interface. Moreover, even for a given capillary and die top geometry, the growth interface isotherm shape will be a function of growth speed because the relative level of heating of the die top by the melt changes with melt flow speed. In the general case, the bulk melt temperature thus becomes an additional variable which may influence interface shape through affecting the temperature of the melt at the capillary exit.

The understanding of the stress and buckling problems rests in gaining more complete knowledge of the vertical and horizontal temperature profiles in the ribbon. Steps in this direction are being taken through utilization of a new temperature profiling method which employs silicon ribbon - carbon thermocouples [16]. Manipulation of the post-growth thermal environment through alterations in the geometry and configuration of the cartridge components responsible for ribbon cooling and reheat can then be related to ribbon stress and buckling patterns in a systematic manner.

Acknowledgements

References

[1] B. H. Mackintosh, T. Surek, J. P. Kalejs, E. M. Sachs, S. Nagy and F. Wald, in: Proc. Thirteenth IEEE Photovoltaic Specialists Conf. (IEEE, New York, 1978) p. 350.

[2] T. Surek, B. Chalmers and A. I. Mlavsky, J. Crystal Growth 42 (1977) 453.

[3] B. Chalmers, H. E. LaBelle, Jr. and A. I. Mlavsky, Mater. Res. Bull. 6 (1971) 681.

[4] K. V. Ravi, J. Crystal Growth 39 (1977) 1.

[5] J. C. Swartz, T. Surek and B. Chalmers, J. Electron. Mater. 4 (1975) 255.

[6] F. V. Wald et. al., First Quarterly Report, ERDA/JPL 954355/78-1 (April, 19 (unpublished).

[7] S. R. Coriell, private communication (1976).

[8] E. Sachs, private communication (1978).

[9] B. A. Boley and J. H. Weiner, Theory of Thermal Stresses (Wiley, New York, 1960), Ch. 14-16.

[10] A. D. Morrison, K. V. Ravi, C. V. Hari Rao, T. Surek, D. F. Bliss, L. C. Garone and R. W. Hogencamp, Fourth Quarterly Report, ERDA/JPL 954355/76-4 (December, 1976) (unpublished).

[11] W. Gurtler, paper appearing in this volume of J. Crystal Growth.

[12] V. G. Ermenko and V. I. Nikitenko, Phys. Stat. Sol. (a) 14 (1972) 317.

[13] S. Timoshenko and S. Woinowsky-Krieger, Theory of Plates and Shells (McGraw-Hill, New York, 1959).

[14] C. V. H. N. Rao, M. C. Cretella, F. V. Wald and K. V. Ravi, paper appearing in this volume of J. Crystal Growth.

[15] J. P. Kalejs, J. Crystal Growth 44 (1978) 329.

[16] E. Sachs, Mobil Tyco Solar Energy Corporation (unpublished research).

TABLE 1

Die top temperature differences calculated from one-dimensional heat transfer model (Eqs. (1) and (2) in text) and ribbon thickness data of fig. 8 for $T_o = 1100^\circ K$, $\epsilon = 0.54$, $k_L = 0.6 \times 10^7$ ergs/sec-cm-$^\circ$K, $k_M = 0.2 \times 10^7$ ergs/sec-cm-$^\circ$K, $\rho L = 4.14 \times 10^9$ ergs/cm^3, and $t_D = 0.066$ cm.

Growth Speed (cm/min)	Average Thickness Measurement Location	Average Thickness (cm)	Meniscus Height (cm)	G_L ($^\circ$C/cm)	$T_D - T_M$ ($^\circ$C)
3.4	ribbon face	0.033	0.036	220	5.6
3.4	ribbon edge	0.056	0.018*	80	1.3
3.8	ribbon face	0.026	0.040	255	6.2
3.8	ribbon edge	0.044	0.020*	95	1.5
4.7	ribbon face	0.020	0.043	248	5.5
4.7	ribbon edge	0.040	0.022*	17	0.3

* Estimated average meniscus height for a region within 0.5 cm of the ribbon edge.

Figure Captions

fig. 1.   Section view of high speed cartridge for 7.5 cm wide ribbon growth.

fig. 2.   Schematic of two piece die used in study of growth stability of
            7.5 cm wide ribbon. Typical die flat widths are 0.005 cm to 0.010
            cm; top slot dimensions range from 0.02 cm to 0.05 cm.

fig. 3.   Schematics of die top cross sections showing several capillary arrange-
            ments: (a) open channel die; (b) distributed capillary die; (c) centra
            capillary die.

fig. 4.   Top view of die and face and end heaters.

fig. 5.   Idealized vertical temperature profiles above die top for static seed-
            ing (case 1) and steady-state growth (cases 2, 3 and 4). Cases are
            discussed in text. T_M is the melting point temperature for silicon.

fig. 6.   Thickness profiles of ribbon for constant width growth with overall die
            top (flats plus slot) width, t_D, of 0.066 cm.

fig. 7.   Variation of isotherm shape across die width: (a) for zero end heater
            power; (b) for steady-state growth.

fig. 8.   Thickness profiles for constant width growth at three growth speeds:
            1. 3.4 cm/min; 2. 3.8 cm/min; 3. 7.7 cm/min. Overall die top (flats
            plus slot) width, t_D, of 0.066 cm was used.

fig. 9.   Sectioned die top showing silicon carbide growth around vertical
            capillary exits in central capillary die.

fig. 10.   Ribbon splitting as a result of high residual stress.

fig. 11.   Buckle patterns observed in 7.5 cm wide ribbon. The surface profile
            traces to the left of each photograph are taken along the growth direc-
            tion of the ribbon shown: (a) edge buckle pattern; (b) center buckle
            pattern.

Figure Captions (cont'd)

fig. 12. Variation of the longitudinal stress σ_{xx} with (a) distance from the growth interface and (b) position across the ribbon width. The stress values are in units of $(\alpha E)^{-1}$, where α is the coefficient of thermal expansion and E is the modulus of elasticity. A quadratic temperature distribution along the ribbon, viz., $T(x) = 56x^2 - 560x + 1685$, and a ribbon width w = 2 cm have been assumed in the calculations.

fig. 13. Schematics of (a) ideal and (b) experimentally determined vertical temperature profiles for high speed cartridge.

fig. 14. (a) Relief of T-C-T longitudinal stress distribution by center buckling. (b) Relief of C-T-C longitudinal stress distribution by edge or torsional buckling.

Fig. 1

Fig. 2

(o) .

(b)

(c)

Fig. 3

FACE HEATER

DIE

END HEATERS
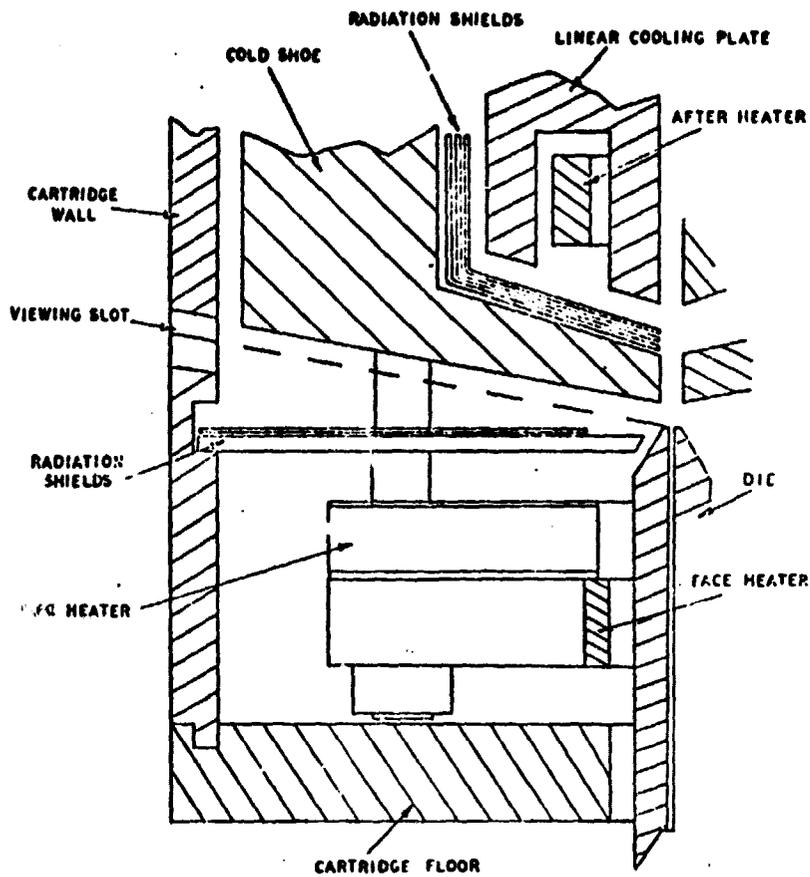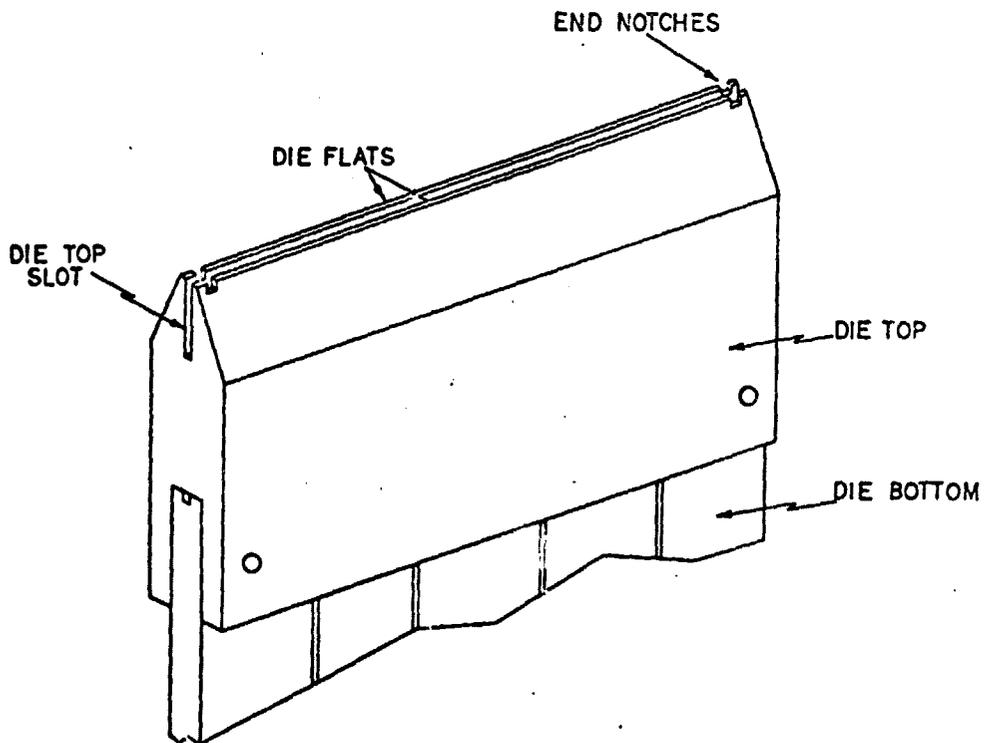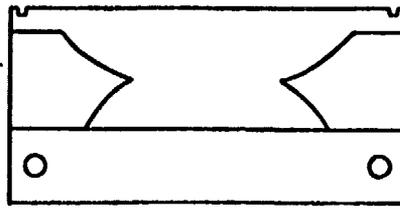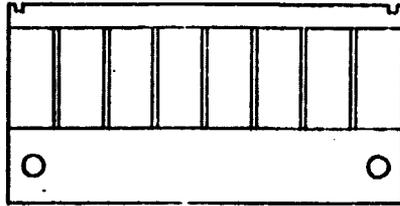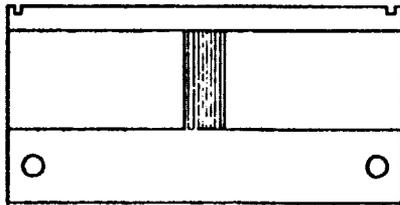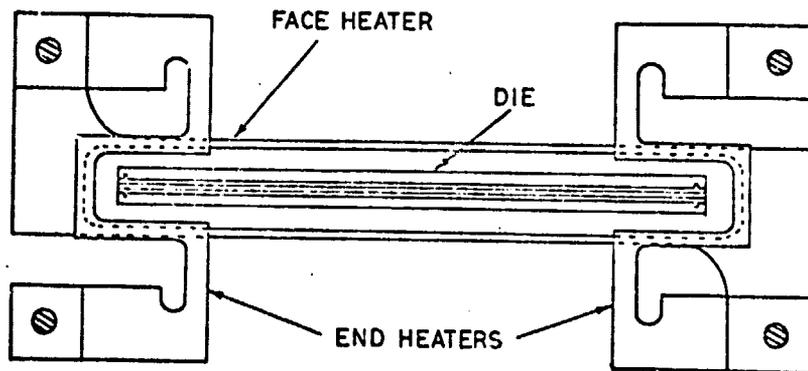
Fig. 4

Fig. 5

Fig. 6

Fig. 7

Fig. 8

Fig. 9

Fig. 10

EDGE   CENTER   EDGE

(a)

EDGE   CENTER   EDGE

(b)

Fig. 11

(a) DISTANCE FROM INTERFACE, X (cm)

(b) DISTANCE ACROSS RIBBON, Y (cm)

Fig. 12

DISTANCE FROM GROWTH INTERFACE ⟶

Fig. 13

$\sigma_{xx} = 0$

$\sigma_{xx} = 0$

(a)   (b)

Fig. 14